Article

Cell

A Viral Immunoevasin Controls Innate Immunity by Targeting the Prototypical Natural Killer Cell Receptor Family

Graphical Abstract

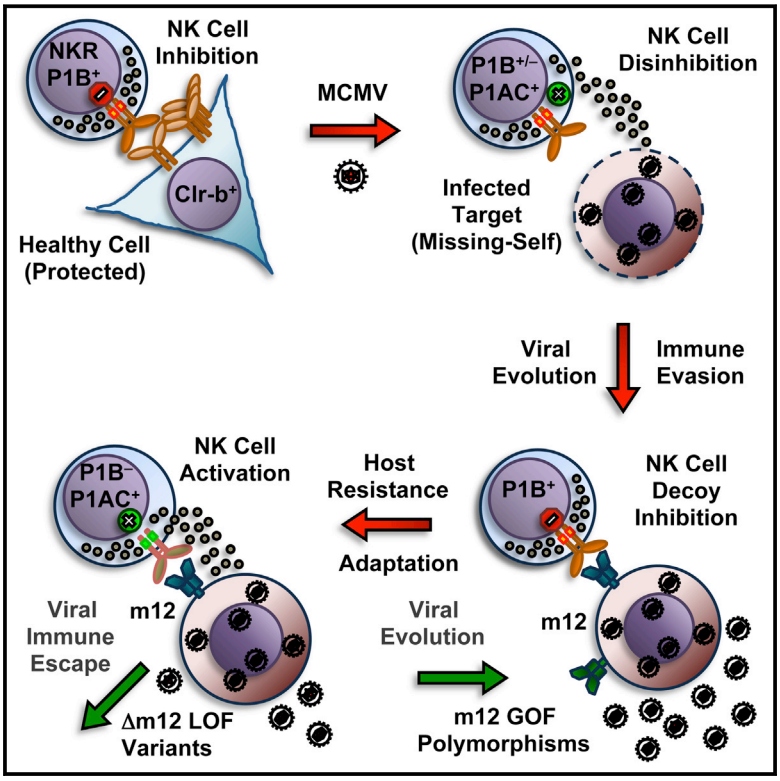

Highlights

- Physiological ligand for the prototypical NK1.1 antigens is an MCMV immunoevasin, m12
- m12 decoy inhibits NK cells via NKR-P1B yet activates via NKR-P1A/C allomorphs
- Crystal structure of mouse NKR-P1B bound to m12 reveals a "polar claw" docking mode
- Co-evolutionary viral m12 and host NKR-P1B/C polymorphisms impact NK responses in vivo

Authors

Oscar A. Aguilar, Richard Berry, Mir Munir A. Rahim, ..., Stipan Jonjić, Jamie Rossjohn, James R. Carlyle

Correspondence

andrew.makrigiannis@dal.ca (A.P.M.), stipan.jonjic@medri.uniri.hr (S.J.), jamie.rossjohn@monash.edu (J.R.), james.carlyle@utoronto.ca (J.R.C.)

In Brief

A viral decoy is the long-sought ligand for a key immunoregulatory receptor family on natural killer cells.

Aguilar et al., 2017, Cell *169*, 58–71
March 23, 2017
http://dx.doi.org/10.1016/j.cell.2017.03.002

CellPress

Cell

Article

A Viral Immunoevasin Controls Innate Immunity by Targeting the Prototypical Natural Killer Cell Receptor Family

Oscar A. Aguilar,[1,2,11] Richard Berry,[3,6,11] Mir Munir A. Rahim,[4,9] Johanna J. Reichel,[5] Branka Popović,[5] Miho Tanaka,[1,2] Zhihui Fu,[3] Gautham R. Balaji,[3,6] Timothy N.H. Lau,[1,2] Megan M. Tu,[4] Christina L. Kirkham,[1,2] Ahmad Bakur Mahmoud,[4,8] Aruz Mesci,[1,2] Astrid Krmpotić,[5] David S.J. Allan,[1,2,10] Andrew P. Makrigiannis,[4,9,*] Stipan Jonjić,[5,*] Jamie Rossjohn,[3,6,7,*] and James R. Carlyle[1,2,12,*]

[1]Department of Immunology, University of Toronto, Toronto, ON M5S 1A8, Canada
[2]Sunnybrook Research Institute, Toronto, ON M4N 3M5, Canada
[3]Infection and Immunity Program, Department of Biochemistry and Molecular Biology, Biomedicine Discovery Institute, Monash University, Clayton, VIC 3800, Australia
[4]Department of Biochemistry, Microbiology, and Immunology, University of Ottawa, Ottawa, ON K1H 8M5, Canada
[5]Department of Histology and Embryology, Faculty of Medicine, University of Rijeka, 51000 Rijeka, Croatia
[6]ARC Centre of Excellence in Advanced Molecular Imaging, Monash University, Clayton, VIC 3800, Australia
[7]Institute of Infection and Immunity, Cardiff University School of Medicine, Heath Park, Cardiff CF14 4XN, UK
[8]College of Applied Medical Sciences, Taibah University, 30001 Madinah Munawwarah, Kingdom of Saudi Arabia
[9]Present address: Department of Microbiology and Immunology, Dalhousie University, Halifax, NS B3H 4R2, Canada
[10]Present address: National Heart, Lung, and Blood Institute, National Institutes of Health, Bethesda, MD 20892, USA
[11]Co-first author
[12]Lead Contact
*Correspondence: andrew.makrigiannis@dal.ca (A.P.M.), stipan.jonjic@medri.uniri.hr (S.J.), jamie.rossjohn@monash.edu (J.R.), james.carlyle@utoronto.ca (J.R.C.)
http://dx.doi.org/10.1016/j.cell.2017.03.002

SUMMARY

Natural killer (NK) cells play a key role in innate immunity by detecting alterations in self and non-self ligands via paired NK cell receptors (NKRs). Despite identification of numerous NKR-ligand interactions, physiological ligands for the prototypical NK1.1 orphan receptor remain elusive. Here, we identify a viral ligand for the inhibitory and activating NKR-P1 (NK1.1) receptors. This murine cytomegalovirus (MCMV)-encoded protein, m12, restrains NK cell effector function by directly engaging the inhibitory NKR-P1B receptor. However, m12 also interacts with the activating NKR-P1A/C receptors to counterbalance m12 decoy function. Structural analyses reveal that m12 sequesters a large NKR-P1 surface area via a "polar claw" mechanism. Polymorphisms in, and ablation of, the viral m12 protein and host NKR-P1B/C alleles impact NK cell responses in vivo. Thus, we identify the long-sought foreign ligand for this key immunoregulatory NKR family and reveal how it controls the evolutionary balance of immune recognition during host-pathogen interplay.

INTRODUCTION

Natural killer (NK) cells are a subset of innate lymphoid cells (ILC) capable of recognizing an array of pathological target cells. As efficient sentinels responsible for the clearance of cancerous, virus-infected, transplanted, antibody-opsonized, and stressed cells, they discriminate between healthy-self, altered-self, and non-self targets through the integration of balanced signals delivered via multiple families of paired germline-encoded NK cell receptors (NKR) (Raulet and Vance, 2006).

Several NKR families have been described, many of which are grouped together in large genomic regions, such as the natural killer gene complex (NKC). In rodents, most NKR are C-type lectin-like proteins encoded within the NKC. These include the Ly49 (*Klra1*) receptors, the CD94/NKG2 (*Klrd1*/*Klrc1*) receptors, the NKG2D (*Klrk1*) receptor, and the NKR-P1 (*Klrb1*) receptors, which interact with genetically-linked C-type lectin-related (*Clr*/*Clec2*) proteins (Kirkham and Carlyle, 2014; Raulet and Vance, 2006).

There exist at least five functional mouse NKR-P1 receptors, three stimulatory isoforms (NKR-P1A,C,F), and two inhibitory isoforms (NKR-P1B,G) (Carlyle et al., 2008; Kirkham and Carlyle, 2014). Originally described almost 40 years ago (Glimcher et al., 1977), the NKR-P1 proteins were the first receptors to be identified as selectively expressed by NK cells. Yet to date, NKR-P1C, the prototypical NK1.1 antigen in B6 mice (Glimcher et al., 1977; Koo and Peppard, 1984; Ryan et al., 1992), and NKR-P1A remain orphan-activating receptors with unknown physiological ligands. On the other hand, the paired NKR-P1F and NKR-P1G receptors recognize overlapping "self" Clr (*Clec2*) ligands to balance signals during NK cell education and effector responses, while the inhibitory NKR-P1B receptor recognizes the broadly expressed self Clr-b (*Clec2d*) ligand (Carlyle et al., 2004; Chen et al., 2011; Iizuka et al., 2003; Kveberg et al., 2009). To date, Clr-b has

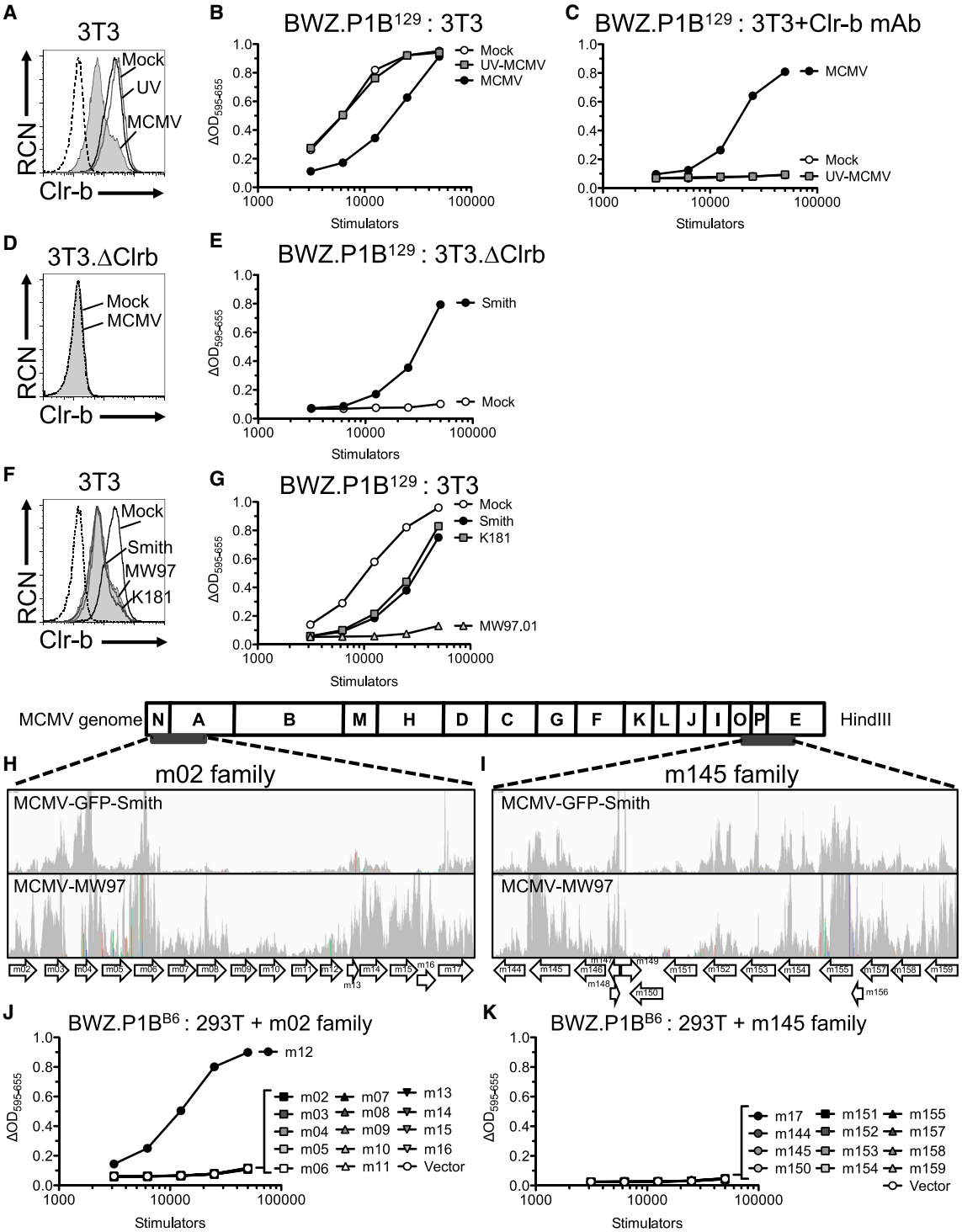

Figure 1. MCMV Encodes a Clr-b-Independent NKR-P1B Immunoevasin, the m02 Family Member, m12

Mouse NIH 3T3 fibroblasts were infected with MCMV^{Smith} overnight and then used as stimulators for BWZ reporter cells expressing a CD3ζ-NKR-P1B^{129} fusion receptor (BWZ.P1B^{129}).

(A) Cell-surface expression of Clr-b on mock, MCMV-infected, or UV-treated MCMV-infected cells.

(B and C) BWZ.P1B^{129} reporter cell assays using the above stimulators in the absence or presence of blocking Clr-b mAb (10 μg/ml).

(D and E) Clr-b-deficient NIH 3T3.ΔClr-b cells, targeted by CRISPR/Cas9 genome editing, analyzed by flow cytometry and BWZ.P1B^{129} reporter assays following MCMV infection.

(legend continued on next page)

been shown to be involved in "missing-self" recognition under diverse pathological states (Kirkham and Carlyle, 2014), including cancer (Carlyle et al., 2004), genotoxic and cellular stress (Fine et al., 2010), hematopoietic transplantation (Chen et al., 2015), immune escape of primary lymphoma cells (Rahim et al., 2015), and cytomegalovirus and poxvirus infection (Aguilar et al., 2015; Voigt et al., 2007; Williams et al., 2012), while the remainder of the self Clr ligands remain less well characterized.

Among pathogens recognized by NK cells, cytomegaloviruses (CMV) demonstrate co-evolution with their natural hosts, likely due to cycles of natural selection for viral versus host fitness. Since early responses to CMV infection are largely NK cell mediated, these viruses have evolved a diverse array of immunoevasins that antagonize NK cell function. For example, the MCMV m157 decoy immunoevasin binds directly to inhibitory Ly49C/I receptors from certain mouse strains, while the stimulatory Ly49H receptor has been evolutionarily adapted to directly recognize m157 as a foreign antigen, in turn dominantly establishing MCMV resistance in B6 mice (Arase et al., 2002).

Here, we identify the MCMV m02 family member, m12, as a functional decoy ligand that directly engages the mouse NKR-P1B inhibitory receptor and inhibits NK cell cytotoxicity. Importantly, we also demonstrate that m12 directly interacts with two stimulatory orphan receptors, the prototypical NK1.1 antigen, NKR-P1C, and NKR-P1A. These findings demonstrate an important role for the NKR-P1 receptor family in NK cell-mediated immunity to infection and identify m12 as the first physiological NKR-P1C^{B6} ligand, almost four decades since its discovery as the prototypical NK1.1 antigen (Glimcher et al., 1977).

RESULTS

MCMV Encodes an NKR-P1B Decoy Immunoevasin

The murine NKR-P1B ligand, Clr-b (*Clec2d*), is rapidly lost in response to cellular infection by diverse viruses (Aguilar et al., 2015; Voigt et al., 2007; Williams et al., 2012). However, MCMV-infected fibroblasts also induce a Clr-b-independent NKR-P1B ligand (Aguilar et al., 2015). To establish whether this was due to a viral immunoevasin, we infected cells with different MCMV strains and used them as stimulators for BWZ.CD3ζ/NKR-P1B^{129} (BWZ.P1B^{129}) reporter cell assays (Mesci and Carlyle, 2007). As shown in Figure 1, mock-treated NIH 3T3 cells or cells exposed to UV-irradiated MCMV strongly stimulated BWZ.P1B^{129} reporter cells, a stimulus that was blocked using Clr-b mAb, while weaker stimulation was observed upon live MCMV^{Smith} infection, which could not be blocked using Clr-b mAb (Figures 1A–1C). Thus, live MCMV infection is required to both downregulate host Clr-b and induce an alternative Clr-b-independent ligand.

To confirm that this signal was Clr-b independent, we generated Clr-b-deficient NIH 3T3 cells (NIH 3T3.ΔClrb) by CRISPR/Cas9-mediated genome editing. Only MCMV-infected, but not mock-treated, NIH 3T3.ΔClrb cells stimulated BWZ.P1B^{129} reporter cells (Figures 1D and 1E). Employing another approach, we compared MCMV infection of primary adult ear fibroblasts (AEF) from B6 WT and B6.*Clr-b*$^{-/-}$ mice (Chen et al., 2015); here, BWZ.P1B^{129} reporter cells responded only to infected B6.*Clr-b*$^{-/-}$ AEF, whereas WT AEF behaved similarly to NIH 3T3 cells (Figures S1A and S1B). Notably, similar results were observed upon MCMV infection of primary *Clrb*$^{-/-}$/β_2*m*$^{-/-}$ AEF cells (Figure S1C) and rat fibroblasts (data not shown). Thus, a Clr-b/β_2m-independent NKR-P1B ligand is induced upon MCMV infection of mouse and xenogeneic rat fibroblasts.

Since NKR-P1B is inhibitory, these results suggest that MCMV may encode a decoy immunoevasin. To test this, we analyzed distinct MCMV strains and large genomic deletion mutants to determine whether any isolates lacked the NKR-P1B reporter signal upon infection. The MCMV^{Smith} and MCMV^{K181} strains both generated strong BWZ.P1B^{129} reporter signals; however, none of the mutants tested nor the parental BAC-generated MCMV^{MW97} strain elicited significant BWZ.P1B^{129} reporter responses (Figures 1F and 1G). This suggested that MCMV^{MW97} might possess a polymorphism or loss-of-function mutation that abrogated BWZ.P1B^{129} reporter cell recognition.

The MCMV-Encoded m12 Immunoevasin Targets NKR-P1B-Mediated Inhibition

To take advantage of the discrepancy between the MCMV strains, we conducted unbiased whole-transcriptome RNA-sequencing (RNA-seq) using MCMV-infected NIH 3T3 cells to identify differences between MCMV^{Smith} and MCMV^{MW97}. RNA-seq reads were then mapped to the MCMV genome sequence using TopHat analysis and visualized using the IGV browser. Since numerous MCMV immunoevasin genes are located at the left or right genomic termini, such as the m02 and m145 families, we analyzed differences within these regions (Figures 1H and 1I). Within the m145 family, few differences in transcript expression or genetic polymorphisms were noted between the two MCMV strains (Tables S1 and S2). In contrast, the m02 family displayed significantly more differences in transcript profiles and single-nucleotide polymorphisms (SNP). To screen these alleles functionally, we independently cloned all of the MCMV^{Smith} m02 and m145 family members and some other known immunoevasins (in total, 32 gene products spanning ~15% of the MCMV genome) into a mammalian expression vector, and then we tested them individually using human 293T transfectants as stimulators for BWZ.P1B^{B6} reporter cells. While none of the m145 family gene products yielded positive results, a single gene product in the m02 family, m12, was capable of directly stimulating BWZ.P1B^{B6}, but not parental BWZ reporter cells (Figures 1J and 1K). Thus, m12 is an NKR-P1B decoy ligand.

(F and G) Cell-surface Clr-b expression and BWZ.P1B^{129} reporter cell assays using NIH 3T3 cells infected with different MCMV strains (Smith, K181, and MW97.01). Data are representative of at least three independent experiments.

(H and I) RNA-seq analysis was performed using RNA from NIH 3T3 cells infected with either MCMV-GFP^{Smith} or MCMV^{MW97}, and the resulting reads were mapped onto the MCMV genome. Histograms from MCMV-GFP^{Smith} (top) and MCMV^{MW97} (bottom) reads mapped to the (H) m02 and (I) m145 regions. SNP are shown as different colored lines in histograms.

(J and K) BWZ.P1B^{B6} reporter cell assays using HEK293T stimulator cells transfected with members of the (J) m02 or (K) m145 families. Data are representative of at least two independent experiments.

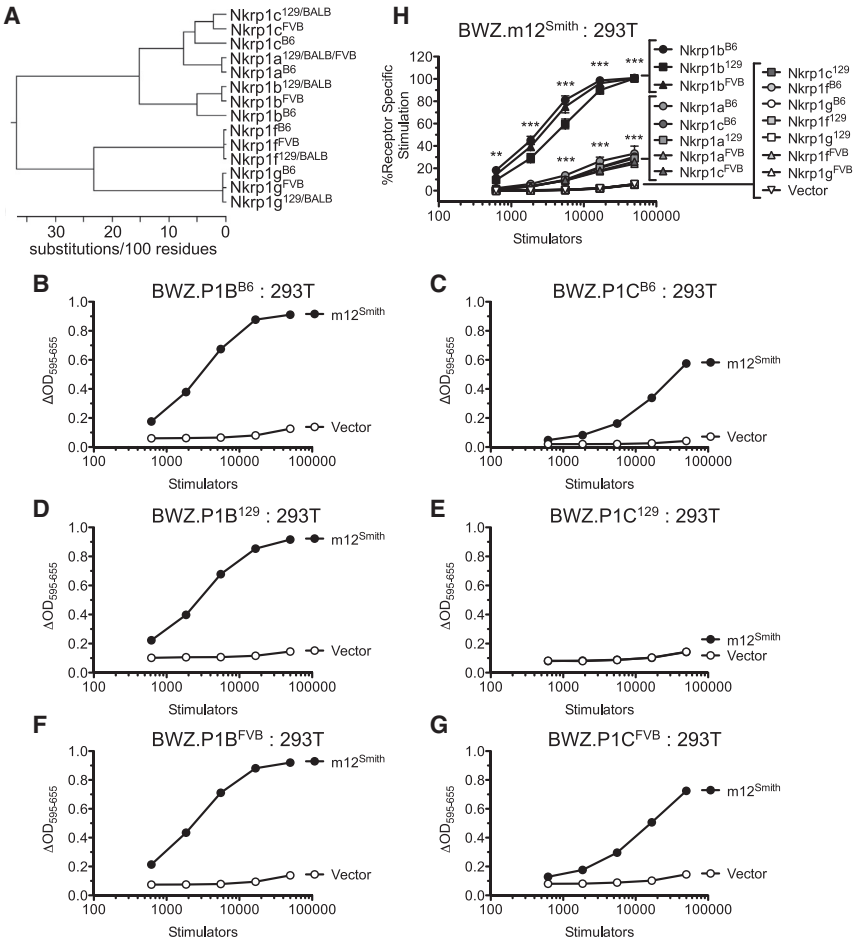

Figure 2. Recognition of m12 by the Stimulatory NKR-P1C/NK1.1 Orphan Receptor

(A) Phylogenetic tree of the NKR-P1 family amino acid sequences from the B6, 129/BALB, and FVB strains using a ClustalW alignment.

(B–G) HEK293T cells transfected with $m12^{Smith}$ were analyzed using BWZ reporter cells bearing the (B) NKR-$P1B^{B6}$, (C) NKR-$P1C^{B6}$, (D) NKR-$P1B^{129}$, (E) NKR-$P1C^{129}$, (F) NKR-$P1B^{FVB}$, or (G) NKR-$P1C^{FVB}$ alleles. Data are representative of at least four independent experiments.

(H) BWZ reporter cells bearing a chimeric m12/CD3ζ fusion receptor (BWZ.m12) were used to analyze HEK293T stimulator cells transfected with NKR-P1 receptors from the B6, 129/BALB, or FVB strains. Data are cumulative from four independent experiments normalized to control values. Mean ± SEM are shown, with significance determined by two-way ANOVA relative to vector control.

m12 Is a Glycosylated Type I Transmembrane Protein

We next characterized the topology, localization, and functional expression of m12. While a transmembrane (TM) domain was identified near the C terminus of m12 (Figure S2A), SignalP did not detect an N-terminal signal peptide. However, bioinformatic analyses identified a second in-frame ATG codon that yielded a canonical signal peptide (when analyzed by SignalP) and translational start site (according to the NetStart server). To validate the second ATG translational initiation site, we generated several m12 constructs, including native m12 ($m12^{ATG1}$, $m12^{ATG2}$) and N-terminal FLAG-tagged m12 with either a native or preprotrypsin signal peptide ($m12^{NSP\text{-}FLAG}$, $m12^{PSP\text{-}FLAG}$). These constructs were then analyzed using 293T transient transfectants, flow cytometry, and BWZ.$P1B^{129}$ reporter cell assays (Figures S2B and S2C).

Notably, cell-surface $m12^{FLAG}$ was detected on transfectants using ATG2 and both signal peptides ($m12^{NSP\text{-}FLAG}$, $m12^{PSP\text{-}FLAG}$), confirming a type I TM topology (Figure S2B). In addition, all of the m12 constructs stimulated BWZ.$P1B^{B6}$ reporter cells, with $m12^{ATG1}$ yielding the weakest signal (Figure S2C). Collectively, these results suggest that ATG2 is preferred, the native signal peptide is cleaved, and m12 is expressed as a functional type I TM cell-surface protein.

To assess m12 biochemically, we conducted immunoprecipitation and western blot analysis of 293T transfectants. Under non-reducing conditions, the m12 protein exists both as a ~35–40 kDa monomer and a ~60–75 kDa dimer (Figure S2D). Under reducing conditions, only a single band of ~40 kDa was observed. Enzymatic digestion using endoglycosidase-H (EndoH) revealed a ~40 kDa EndoH-resistant band and a ~28 kDa EndoH-sensitive band, while treatment with peptide-N-glycosidase-F (PNGaseF) demonstrated a single band at ~28 kDa, in accordance with a predicted size of 24.6 kDa. These data suggest that m12 is a highly N-linked glycosylated type I TM protein.

Recognition of m12 by the Prototypical NK1.1 Activating Receptor, NKR-$P1C^{B6}$

We next tested whether m12 was capable of interacting with paralogous host receptor isoforms and alleles. To this end, BWZ reporter cells bearing CD3ζ-fusion NKR-P1A/B/C/F/G receptors were constructed from the FVB, B6, and 129/BALB-strain alleles. Notably, the NKR-$P1B^{FVB}$ and NKR-$P1C^{B6}$ alleles react with NK1.1 mAb, whereas the NKR-$P1B^{129/BALB}$ alleles do not (Carlyle et al., 1999, 2006; Ryan et al., 1992), and NKR-P1A/B/C forms a separate clade from NKR-P1F/G (Figure 2A).

When BWZ.NKR-P1 reporter cells were stimulated using 293T transfectants of the $m12^{Smith}$ allele, the stimulatory NKR-P1A, NKR-P1F, and inhibitory NKR-P1G receptors did not appreciably recognize $m12^{Smith}$ (data not shown), while all inhibitory NKR-P1B receptor alleles recognized $m12^{Smith}$ (Figures 2B, 2D, and 2F). Remarkably, the $m12^{Smith}$ immunoevasin also significantly interacted with the stimulatory NKR-$P1C^{B6}$ receptor, demonstrating that $m12^{Smith}$ is a much-anticipated natural ligand for the prototypical NK1.1 antigen (Glimcher et al., 1977; Koo and Peppard, 1984; Ryan et al., 1992) (Figure 2C).

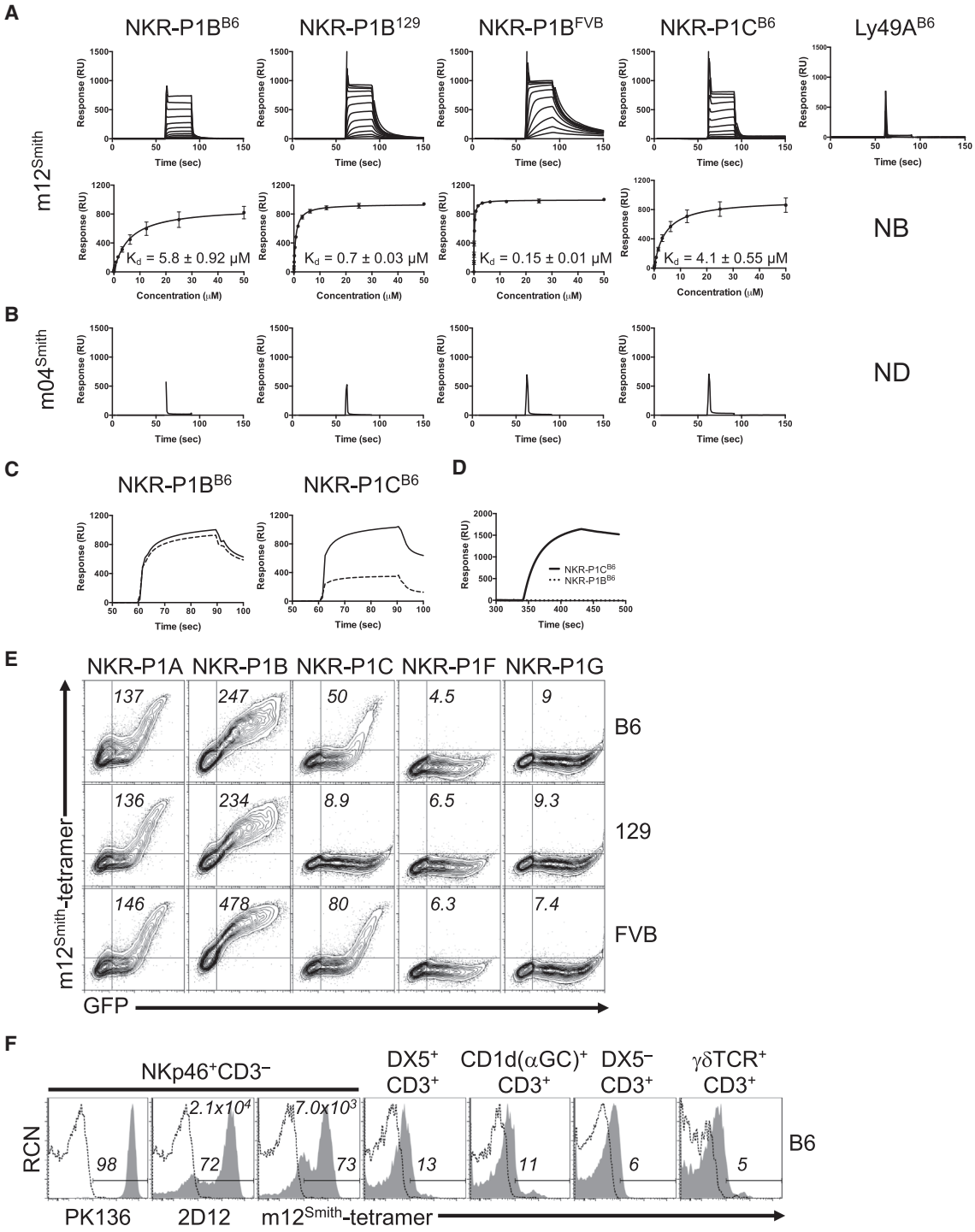

Figure 3. Direct Binding of m12 Protein to NKR-P1 Receptors

(A and B) Surface plasmon resonance sensograms and equilibrium binding curves (where appropriate) are shown for the binding of (A) $m12^{Smith}$ (0.025–50 μM) and (B) $m04^{Smith}$ (100 μM) to various NKR-P1 or Ly49 receptors, as indicated. Equilibrium dissociation constants (K_d) were calculated from two independent measurements, with each experiment performed in duplicate. Error bars represent the SEM. NB, no binding; ND, not determined.

(C) Sensograms are shown for the binding of 50 μM $m12^{Smith}$ to $NKR\text{-}P1B^{B6}$ and $NKR\text{-}P1C^{B6}$ either before (solid lines) or after (dashed lines) exposure of immobilized receptor to the NK1.1 antibody.

(D) The relative binding of NK1.1 mAb to immobilized $NKR\text{-}P1B^{B6}$ and $NKR\text{-}P1C^{B6}$.

(E) $m12^{Smith}$ tetramer binding to HEK293T cells transfected with NKR-P1 alleles from B6, 129, and FVB strains. Numbers correspond to mean fluorescence intensities of the GFP^+ gate.

(legend continued on next page)

Interestingly, the NK1.1^{-} NKR-P1C^{FVB} allele also recognized m12^{Smith}, but the NK1.1^{-} NKR-P1C$^{129/BALB}$ allele did not (Figures 2E and 2G), demonstrating that paralogous stimulatory recognition of m12^{Smith} is not unique to B6 mice.

To confirm these results reciprocally, we also generated BWZ.m12^{Smith} reporter cells and used them to semiquantitatively assess interactions with all NKR-P1 alleles on 293T transfectants (Figure 2H). Using this approach, BWZ.m12^{Smith} reporters recognized NKR-P1B^{B6,129,FVB}, NKR-P1A$^{B6,129/FVB}$, and NKR-P1C^{B6,FVB}, but not NKR-P1C^{129}; however, the stimulatory NKR-P1A/C paralogs interacted with m12^{Smith} more weakly than the inhibitory NKR-P1B counterparts in this cellular context. This was not due to splice variants nor inefficient surface expression of the stimulatory isoforms, as reciprocal domain swaps of NKR-P1B and NKR-P1C stimulated m12^{Smith} reporters similarly to native isoforms (Figures S2E and S2F). Collectively, dual recognition of m12 by paralogous NKR-P1 receptors with opposing signals suggests that NKR-P1:m12 interactions are evolving under selection pressures driven by host-pathogen interactions.

Direct Interactions between the NKR-P1A/B/C and m12 Proteins

Next, we expressed soluble m12 and NKR-P1 receptor ectodomains and assessed their interaction by surface plasmon resonance (SPR). Here, m12^{Smith} bound with similar affinity to the inhibitory NKR-P1B^{B6} (K_d = 5.8 μM) and stimulatory NKR-P1C^{B6} (K_d = 4.1 μM) receptors (Figure 3A). As observed using reporter cell assays, m12 recognition was found to be highly allele sensitive, with m12^{Smith} binding to NKR-P1B^{129} and NKR-P1B^{FVB} with affinities 8-fold (K_d = 0.7 μM) and 40-fold (K_d = 0.15 μM) higher than observed for NKR-P1B^{B6} (Figure 3A). As controls, m12^{Smith} did not bind to the structurally related Ly49A^{B6} receptor and m04 did not bind appreciably to any NKR-P1 alleles tested (Figure 3B). Notably, binding of m12^{Smith} to NKR-P1C^{B6}, but not NKR-P1B^{B6}, could be blocked using NK1.1 mAb (Figure 3C), which only recognizes NKR-P1C^{B6} (and NKR-P1B^{FVB}) but not NKR-P1B^{B6} (Figure 3D) (Carlyle et al., 1999, 2006; Ryan et al., 1992).

We further generated m12^{Smith} tetramers and used these to stain transient 293T.NKR-P1 transfectants using an IRES-GFP reporter vector. These m12 tetramers were found to bind directly to cells expressing NKR-P1A^{B6,129,FVB}, NKR-P1B^{B6,129,FVB}, and NKR-P1C^{B6,FVB}, but not NKR-P1C^{129}, NKR-P1F, or NKR-P1G (Figure 3E). Notably, m12^{Smith} tetramer staining of the activating NKR-P1A/C receptors was significantly lower than for the inhibitory NKR-P1B receptors at similar IRES-GFP reporter levels, indicating a weaker avidity of m12^{Smith} for the cellular NKR-P1A/C isoforms. In addition, the m12^{Smith} tetramers bound to fresh ex vivo B6-strain lymphocyte subsets, which mainly consisted of the NKR-P1B^{+} subset of NK cells, with significantly lower staining observed for the remaining NK cells, NKT cells, and T cells, likely due to the weaker m12:NKR-P1A/C interactions at the cell surface (Figure 3F). Interestingly, differential results were observed for ex vivo lymphocytes from a number of distinct mouse strains (B6.*Clr-b*$^{-/-}$, 129, BALB/c, FVB; Figure S3A), suggesting that differential susceptibility to MCMV m12 variants might be expected.

Reciprocally, we also generated NKR-P1B tetramers from the B6, 129, and FVB strains and used these to stain m12-expressing cells. Here, NKR-P1B^{B6,129,FVB} tetramers variably stained transient 293T.m12 and 293T.Clr-b transfectants, stable BWZ.m12 transductants, and NIH 3T3 cells infected with MCMV variants, demonstrating their utility in the absence of m12 mAb (Figures S3B–S3C and data not shown). Importantly, differences in NKR-P1 tetramer staining levels were observed using distinct NKR-P1 receptors across several m12 variants from distinct MCMV strains; these differences likely reflect their respective avidities for m12 variants at the cell surface (as they follow a similar affinity hierarchy to SPR results, where FVB > 129 > B6 for m12^{Smith}; see also below). Collectively, the above results demonstrate that there exists allelic and isoform specificity among the direct m12:NKR-P1A/B/C protein-protein interactions.

Structure of m12^{Smith} Complexed to NKR-P1B^{B6}

We next determined the structure of NKR-P1B^{B6} bound to m12^{Smith} (Figure 4; Figure S4; Table S3). NKR-P1B adopted a classical C-type lectin-like domain (CTLD) fold and possessed a compact β3-β4 loop rather than the extended conformation observed in murine NKR-P1A (Kolenko et al., 2011) (Figure S4A). Overall, m12 adopts an eight-stranded β-sandwich fold comprising one large (AIDEF) and one small (BGHC) β sheet, similar to that described for the m04 immunoevasin (Figures S4B–S4D) (Berry et al., 2014; Sgourakis et al., 2014). Like m04, the m12 I strand possesses two cysteine residues (Cys168 and Cys173) that form intra-molecular disulfide bonds with the CD loop (Cys88) and A strand (Cys58), respectively. However, m12 also contains an additional disulfide bridge between Cys40-Cys95 that serves to tether the relatively long N-terminal extension to the CD loop (Figure S4). Moreover, m12 possesses an additional α helix between the B and C strands. Thus, m12 possesses unique structural features that are directly involved in NKR-P1B receptor binding.

Topologically, m12 lies across the top of the NKR-P1B CTLD, such that the m12 β sheets lie parallel to the interface (Figure 4A). Here, m12 straddles NKR-P1B in a claw-like manner, whereby a relatively flat "palm" engages the planar top surface of the NKR-P1B CTLD, while several "fingers" grasp around the periphery (Figures 4B–4C). This binding mode results in an extensive interface that buries a total solvent-accessible surface area of 2,180 Å^2, which is considerably larger than the 1,680 Å^2 observed upon binding of the KACL endogenous ligand to the human NKp65 receptor (Li et al., 2013) (Figures S4E and S4F).

(F) m12^{Smith} tetramer binding to ex vivo splenocytes from B6 mice gated as indicated: NK cells (NKp46^{+}CD3^{-}); NKT cells (DX5^{+}CD3^{+} or CD1d(αGalCer) tetramer^{+}CD3^{+}); conventional T cells (DX5^{-}CD3^{+}); γδ T cells (γδTCR^{+}CD3^{+}). Numbers above gates indicate percentage of positive cells; numbers at top right corner represent the median fluorescence intensity of cells positive for 2D12 or m12 tetramer (see also Figure S3A). Specific staining, shaded histograms; fluorescence minus one (FMO) control, dashed lines. Data shown are representative of at least two independent experiments.

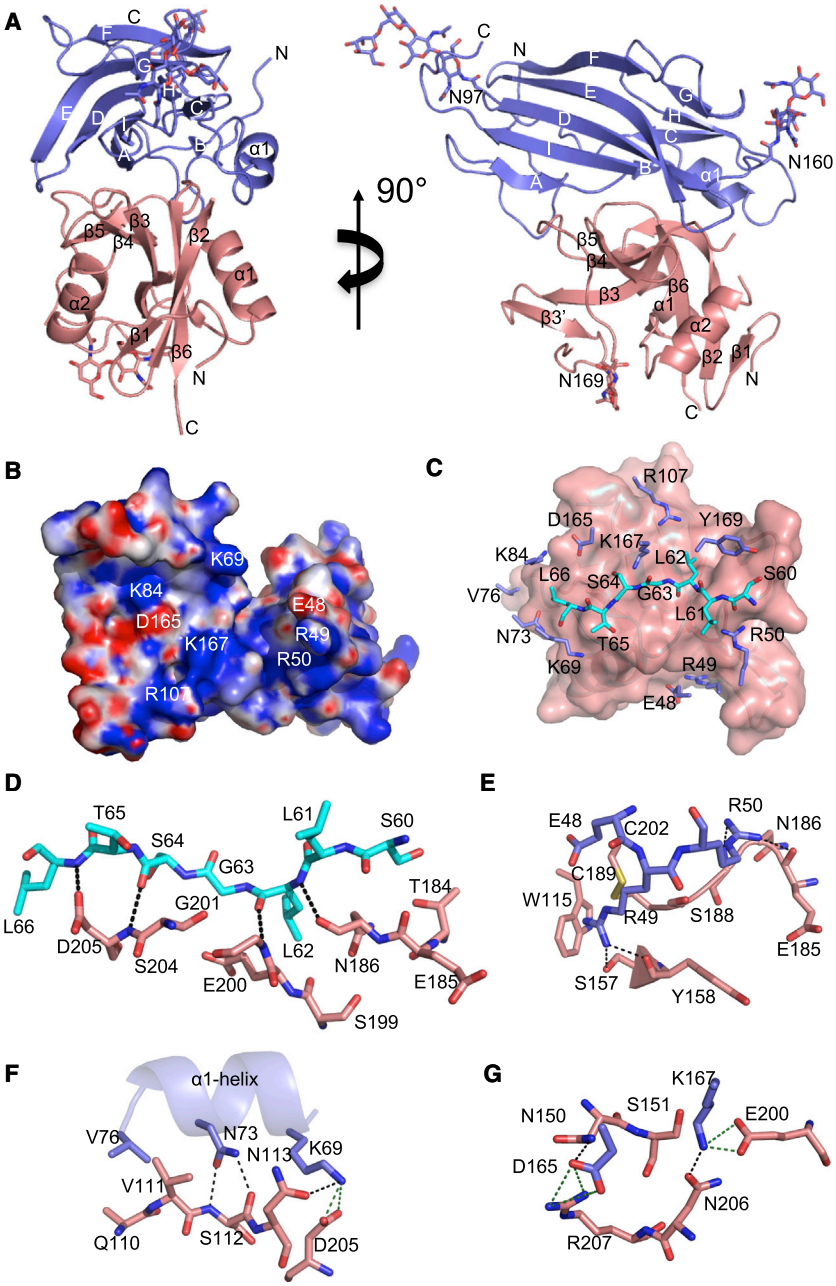

Figure 4. Structure of the m12:NKR-P1B Complex

(A) Overview of m12^{Smith} (blue) bound to NKR-P1B^{B6} (salmon) in cartoon representation. Sugar moieties are shown as sticks.

(B) Positive (blue) and negative (red) electrostatic potentials are shown on the surface of m12 that binds to NKR-P1B.

(C–G) Top view of the m12/NKR-P1B interface. m12 residues that form the "palm" (cyan sticks) and "fingers" (blue sticks) are shown relative to the NKR-P1B surface. Selected interactions between NKR-P1B and the m12 "palm" (D) and "fingers" (E–G). H-bonds and salt-bridges are shown as black and green dashed lines respectively.

The interface is characterized by high shape complementarity and is dominated by hydrophilic interactions, including 14 H bonds and 8 salt-bridges (Figure 4B and Table S4). The m12 palm encompasses residues from the A and B strands as well as the interconnecting loop (Ser60-Leu66) that form an extended surface that simultaneously engages the β2-β3 and β4-β5 loops as well as the β4 strand of NKR-P1B. Here, the interaction is stabilized by a number of H bonds that are primarily derived from the m12 and NKR-P1B main chains (Figures 4C–4D). In contrast to the flat, featureless palm, the m12 fingers are comprised of multiple large, primarily polar residues that form highly specific interactions around the edges of the docking site (Figures 4C and 4E–4G). For example, the m12 N terminus contains a highly charged $_{48}$ERR$_{50}$ motif that flanks the NKR-P1B CTLD (Figure 4E). In addition, the loop region connecting the NKR-P1B β1 sheet to the α1 helix is similarly flanked by a triad of residues (Lys69, Asn73, Val76) that emanate from the unique m12 α1 helix (Figure 4F). Further polar interactions are centered on the base of the m12 I strand, where Asp165 and Lys167 extend downward in order to engage Glu200, Asn206, Arg207, and Asn150 (Figure 4G). Overall, the breadth and the polar claw style of the interactions with NKR-P1B underlie the capacity of m12 to target this receptor family.

A Single Allelic SNP between m12$^{Smith/MW97}$ Impacts NKR-P1B Immunoevasin Function

Despite differential stimulation of BWZ.P1B^{129,B6} reporter cells by NIH 3T3 fibroblasts infected using MCMV^{Smith} versus MCMV^{MW97} (Figure 1G), quantitation of m12 transcripts by qRT-PCR revealed similar mRNA levels between the two viruses (Figure 5A). However, a single G271A SNP was observed in m12^{MW97} that resulted in a non-conservative E91K charge substitution. To determine whether this allelic m12 SNP affected immunoevasin function, we compared BWZ.P1B^{B6} reporter stimulation by m12^{MW97} versus m12^{Smith} in 293T transfectants; indeed, m12^{MW97} was recognized more weakly than m12^{Smith} and host Clr-b (Figure 5B). This suggests that m12^{Smith} is a superior NKR-P1B immunoevasin versus m12^{MW97}, at least in B6 mice. Importantly, this finding was confirmed and extended using NKR-P1B tetramers, whereby all three allelic NKR-P1B^{B6,129,FVB} tetramers stained transient 293T.m12^{Smith} transfectants better than 293T.m12^{MW97} transfectants (Figure S3B).

We further validated these results using cytotoxicity assays. Here, we generated stable retroviral transductant YAC-1 target cells expressing native m12^{Smith}, m12^{MW97}, or host Clr-b

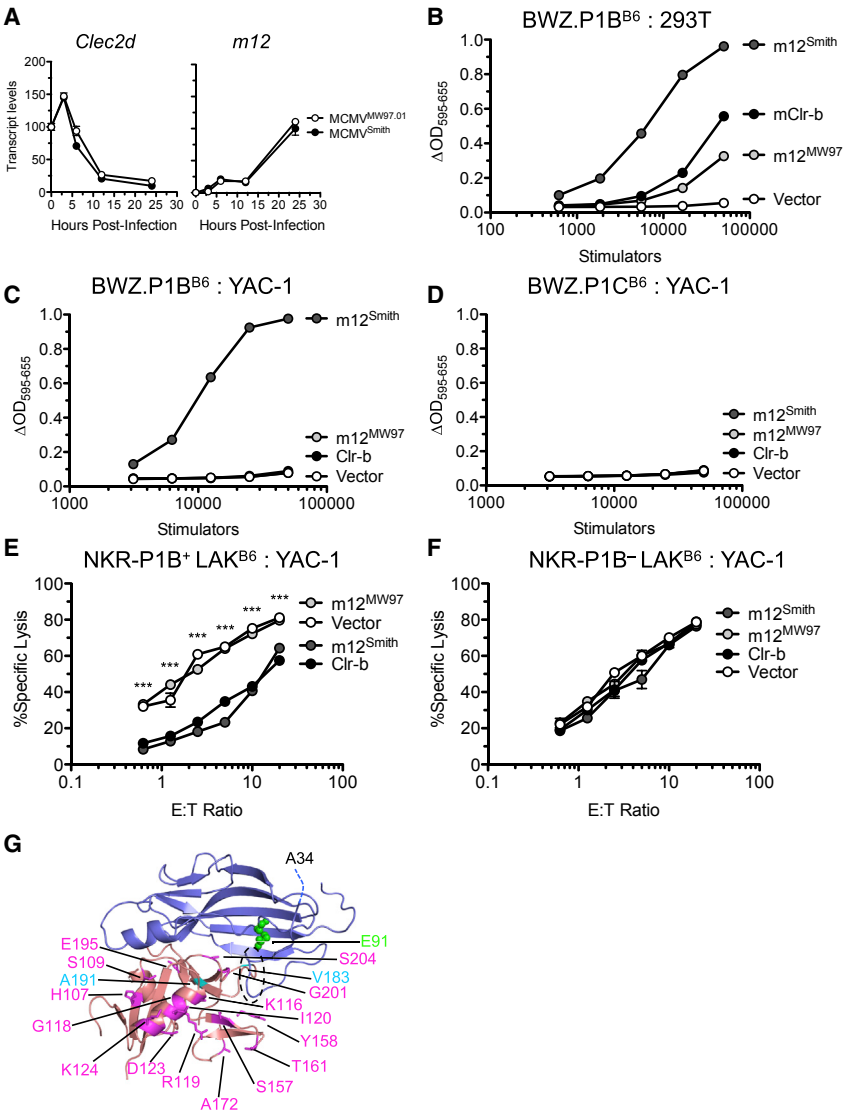

Figure 5. An Allelic MCMV m12 Polymorphism Controls NKR-P1B-Mediated Recognition and Inhibition of Cytotoxicity

(A) Quantitative real-time RT-PCR analysis of host *Clec2d* and MCMV *m12* transcript expression during infection of NIH 3T3 cells with $MCMV^{Smith}$ or $MCMV^{MW97}$.

(B) BWZ.P1B^{B6} reporter cell analysis of HEK293T stimulators transfected with host Clr-b, $m12^{Smith}$, $m12^{MW97}$, or empty vector.

(C and D) YAC-1 cells transduced with $m12^{Smith}$, $m12^{MW97}$, Clr-b, or empty vector were used as stimulators for BWZ.P1B^{B6} or BWZ.P1C^{B6} reporter cells.

(E and F) YAC-1 transductants as above were used as targets in ^{51}Cr-release cytotoxicity assays with sorted NKp46^{+}NKR-P1B^{+} or NKp46^{+}NKR-P1B^{-} NK-LAK effectors. Data are representative of at least two independent experiments. Mean ± SEM values are shown, with pairwise significance determined by two-way ANOVA.

(G) Mapping of polymorphisms on the m12:NKR-P1B structure. Residues that differ between NKR-P1B^{B6} and NKR-P1B^{129} are shown in pink, whereas those that differ between NKR-P1B^{129} and NKR-P1B^{FVB} are shown in cyan. The E91K polymorphism identified in $m12^{MW97}$ is highlighted in green, and the likely position of the A34V substitution found in $m12^{C4A}$ is indicated in black. The m12 $_{48}$ERR$_{50}$ motif is denoted by a dashed oval.

(indexed via IRES-GFP levels; Figure S5A). As observed using 293T transfectants, BWZ.NKR-P1 reporter analyses using YAC-1 stimulators show that BWZ.P1B^{B6} cells recognize $m12^{Smith}$ more strongly than $m12^{MW97}$ (Figure 5C). In contrast, BWZ.P1B^{FVB} cells recognize $m12^{Smith}$ and $m12^{MW97}$ similarly (Figure S5B), suggesting that the energetic profile of the interaction is allele specific. However, we could not detect significant stimulation of BWZ.P1C^{B6} reporter cells using YAC-1.$m12^{Smith}$ stimulators (Figure 5D), perhaps due to the lower m12 expression levels on these sorted stable transductants; notably, these data are consistent with reduced m12 tetramer staining of NKR-P1A/C relative to NKR-P1B (Figure 3E).

Next, YAC-1 transductants were incubated as targets with sorted NKp46^{+}NKR-P1B^{+} or control NKp46^{+}NKR-P1B^{-} B6-strain lymphokine-activated killer (NK-LAK) effectors in ^{51}Cr-release cytotoxicity assays. As shown in Figure 5, YAC-1.$m12^{MW97}$ target cells were killed equivalently to control YAC-1(–) targets, while both YAC-1.$m12^{Smith}$ and YAC-1.Clr-b target cells significantly inhibited NKR-P1B^{+} NK-LAK cell cytoxicity (Figure 5E). Importantly, inhibition by $m12^{Smith}$ and host Clr-b was mediated via NKR-P1B^{B6}, as it was not observed using NKR-P1B^{-} NK-LAK effectors (Figure 5F). Notably, similar results were observed using sorted FVB-strain NKR-P1B^{+} and NKR-P1B^{-} NK-LAK effectors, partitioned using NK1.1 mAb (PK136), which recognizes NKR-P1B^{FVB} (but not NKR-P1C^{FVB}) (Carlyle et al., 1999) (Figures S5C and S5D). The similar recognition of $m12^{Smith}$ and $m12^{MW97}$ using BWZ.P1B^{FVB} reporters (Figure S5B) and NKR-P1B^{FVB} tetramers (Figure S3B) but strong inhibition of cytotoxicity only by $m12^{Smith}$ suggests differential recognition of the m12 alleles by other stimulatory receptors, such as the NKR-P1A/C paralogs (Figure 2H; see also below).

The $m12^{Smith}$:NKR-P1B^{B6} structure provided an opportunity to understand the molecular basis underpinning the highly allele-sensitive nature of this pivotal interaction. For example, NKR-P1B^{129} differs from NKR-P1B^{B6} by 16 residues within the CTLD, but only 4 contact $m12^{Smith}$ (S157R, Y158F, G201S, and S204T). Of these, the S157R and G201S polymorphisms would likely result in additional contacts with $m12^{Smith}$ and would thereby account for the marked increase in affinity of NKR-P1B^{129} compared to NKR-P1B^{B6} (Figure 5G). In addition, the polymorphic m12 residue, E91, did not directly contact NKR-P1B^{B6} but instead packed tightly against the m12 N terminus, thereby facilitating the interaction of the m12 $_{48}$ERR$_{50}$ motif

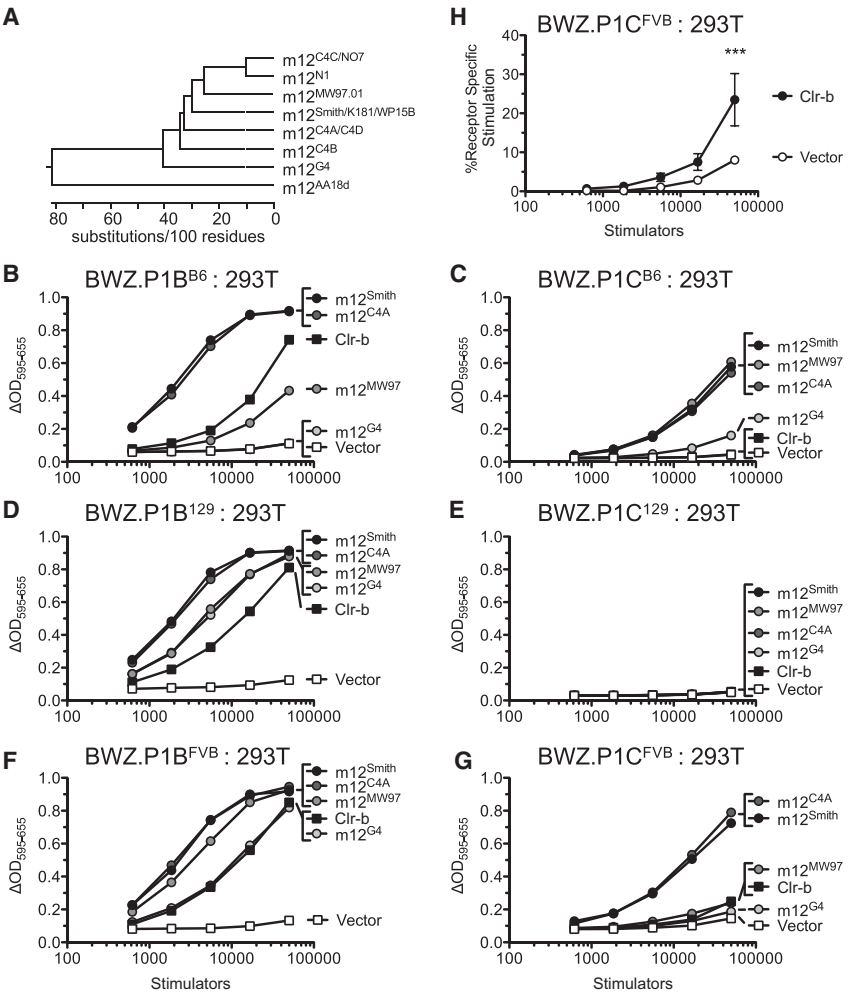

Figure 6. Wild-Derived Isolates of MCMV Show Host-Driven Evolution of the m12 Gene Product

(A) Phylogenetic tree of allelic m12 amino acid sequences derived from sequenced MCMV strains (Smith, K181, MW97.01, WP15B, C4A, C4B, C4C, C4D, G4, AA18d, NO7, and N1).

(B–G) Unique m12 alleles (Smith, MW97, C4A, and G4) were cloned into the pIRES2-EGFP vector, and HEK293T transfectants were used as stimulators for (B) BWZ.P1B^{B6}, (C) BWZ.P1C^{B6}, (D) BWZ.P1B^{129}, (E) BWZ.P1C^{129}, (F) BWZ.P1B^{FVB}, and (G) BWZ.P1C^{FVB} reporter cells. Data are representative of at least three independent experiments.

(H) BWZ.P1C^{FVB} reporter cells stimulated using 293T.Clr-b transfectants; cumulative mean ± SEM from four independent experiments is shown. Significance was determined by two-way ANOVA relative to vector control.

with NKR-P1B^{B6} (Figure 5G). Here, the m12^{MW97} E91K polymorphism would likely disrupt this packing and would thus indirectly abrogate the m12^{MW97}:NKR-P1B^{B6} interaction.

Collectively, these data demonstrate that an allelic m12^{MW97} SNP results in less-efficient NKR-P1B immunoevasin function, while the m12^{Smith} immunoevasin is capable of effective inhibition of both B6 and FVB NK-LAK effectors using YAC-1 targets. Moreover, the crystal structure provides a molecular basis for understanding the impact of host and viral allelic variation across the m12:NKR-P1B axis.

Wild MCMV Isolates Demonstrate Host-Driven Evolution of the m12 Gene Product

The above findings support the existence of both host- and pathogen-driven evolutionary selection pressures, including the loss-of-function m12^{MW97} SNP. Since NKR-P1B and NKR-P1C are polymorphic between mouse strains, we investigated whether additional m12 polymorphisms also exist in wild-derived MCMV isolates. Thus, we searched databases to compare m12 sequences from additional MCMV strains, including the Smith, K181, MW97.01, WP15B, C4A, C4B, C4C, C4D, G4, AA18d, N1, and NO7 isolates (Smith et al., 2013); notably, with the exception of K181 and WP15B, each of the other strains differed from the m12^{Smith} allele by at least one amino acid substitution (MW97.01, C4A/D/B), with extensive polymorphisms observed for some wild isolates (G4), including loss of signal peptide (AA18d), and premature truncations in the m04-like domain (C4C,N1,NO7) (Figure 6A; Figure S6).

To assess these functionally, we cloned unique m12 gene products and then tested their recognition using BWZ.NKR-P1 reporters and 293T.m12 transfectant stimulators. We observed differences in recognition among all MCMV m12 alleles when tested against the different NKR-P1B and NKR-P1C alleles (Figures 6B–6G). The m12^{C4A} variant has an A34V substitution yet engaged all NKR-P1B alleles similarly to m12^{Smith} (Figures 6B, 6D, and 6F); this was also true using NKR-P1B tetramers (Figure S3B). This result is not surprising, since the most N-terminal m12 residue visible in the structure (S39) is distal to the NKR-P1B binding site (Figure 5G). The m12^{MW97} variant, as observed previously, has an E91K substitution and engaged NKR-P1B^{B6} much less efficiently than m12^{Smith} in both reporter assays and using NKR-P1B tetramers, yet this difference was reduced using the NKR-P1B^{129} allele and was absent using the NKR-P1B^{FVB} allele (Figures 6B, 6D, and 6F; Figure S3B). The highly diversified m12^{G4} variant was not recognized by NKR-P1B^{B6}, interacted with NKR-P1B^{129} similarly to m12^{MW97}, and interacted with NKR-P1B^{FVB} less well than other m12 variants (Figures 6B, 6D, and 6F; Figure S3B).

When tested against the NKR-P1C paralogs, all m12 variants interacted with NKR-P1C^{B6} to some extent, although m12^{G4} recognition was very weak (Figure 6C). None of the m12 variants were found to interact with NKR-P1C^{129} (Figure 6E), which may not be functionally expressed, due to the absence of a key cysteine residue (C122S) likely to be involved in intra-molecular stabilization. In contrast, NKR-P1C^{FVB} was stimulated strongly

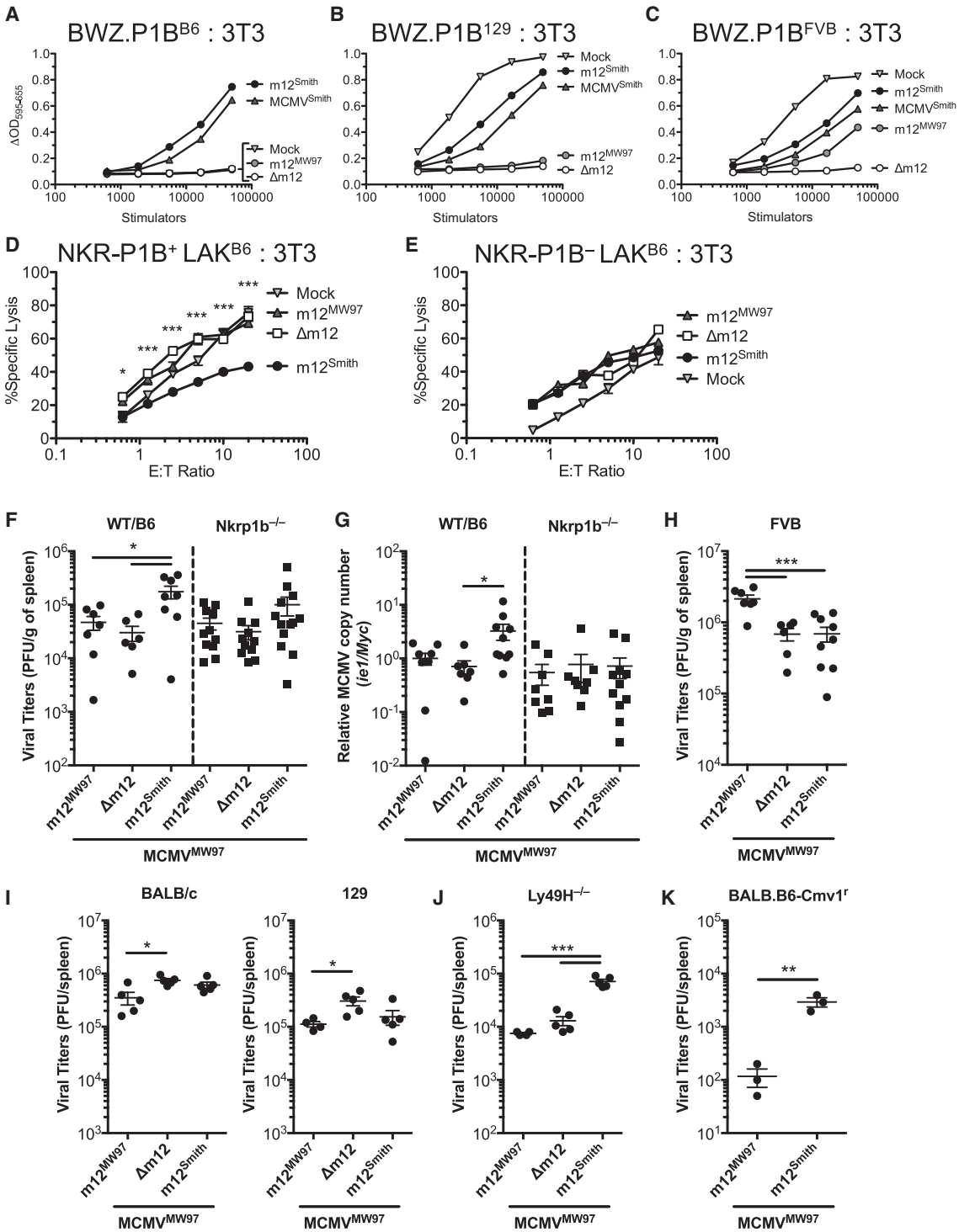

Figure 7. In Vitro and In Vivo Analyses of MCMV m12 Allelic Variants in Distinct Inbred, Congenic, and Mutant Mouse Strains

(A–C) NIH 3T3 fibroblasts were infected with MCMV^{Smith} or parental MW97-strain variants, including WT (m12^{MW97}), Δm12 mutant (Δm12), and m12^{Smith} revertant (m12^{Smith}) then used as stimulators for (A) BWZ.P1B^{B6}, (B) BWZ.P1B^{129}, and (C) BWZ.P1B^{FVB} reporter cells.

(D and E) NIH 3T3 fibroblasts infected with the above MCMV variants were used as targets in ^{51}Cr-release cytotoxicity assays with sorted (D) NKR-P1B^{+} or (E) NKR-P1B^{-} B6-strain splenic NK-LAK effectors.

(F) Viral PFU titers in spleens of WT B6 and B6.*Nkrp1b*$^{-/-}$ mice infected in vivo using the above MCMV variants, analyzed 3 days post-infection. Data are pooled from two independent infections using 1x10^{6} PFU/mouse.

(legend continued on next page)

by m12^{Smith} and m12^{C4A} but very weakly by m12^{MW97} and m12^{G4} (Figure 6G), in turn suggesting that m12^{Smith} immunoevasin function may be counterbalanced by host NKR-P1C^{FVB} activation relative to m12^{MW97} (see also below). Notably, NKR-P1B^{B6} and NKR-P1C^{FVB} only differ in a single m12 contact residue (S204T), thereby explaining their similar responses to the m12 variants (Figure 5G). Interestingly, Clr-b also weakly stimulated NKR-P1C^{FVB} reporters (Figures 6G and 6H), demonstrating that host Clr-b represents a novel activating self NKR-P1C ligand in the FVB strain. These data provide further evidence of the existence of host- and pathogen-driven evolution of the viral m12 decoy and reciprocal host adaptation of the NKR-P1B/C paralogs. These findings also validate the hypothesis that the NKR-P1B/C receptors have been co-evolving as a paired receptor clade to recognize similar host and viral ligands.

MCMV Mutants Reveal NKR-P1B-Dependent Inhibition In Vitro and Virulence In Vivo

To establish an immunoevasin role for m12, we generated m12-modified variants of the parental MCMV^{MW97} strain, including both m12-deficient (Δm12) and m12^{Smith}-revertant (m12^{Smith}) mutants. In vitro characterization revealed that all three MCMV variants similarly downregulated host Clr-b upon infection of NIH 3T3 cells (Figure S7A).

Using infected NIH 3T3 cells directly, the m12^{Smith}-revertant virus stimulated BWZ.P1B^{B6} reporters similarly to the original MCMV^{Smith} virus, while the Δm12 mutant, parental MCMV^{MW97}, and mock-infected NIH 3T3 cells lacked significant stimulation (notably, BWZ.P1B^{B6} reporters routinely fail to recognize endogenous host Clr-b levels on NIH 3T3 cells; Figure 7A). In contrast, using BWZ.P1B^{129} reporters, strong stimulation was observed with MCMV^{Smith} virus, m12^{Smith}-revertant virus, and mock-infected NIH 3T3 cells, compared with weak stimulation using parental MCMV^{MW97}, and no stimulation using Δm12 mutant MCMV (Figure 7B). Finally, using BWZ.P1B^{FVB} reporter cells, stimulation was observed using mock-infected cells, m12^{Smith}-revertant virus, MCMV^{Smith}, and MCMV^{MW97}, but not the Δm12 mutant virus (Figure 7C). The Clr-b-independent nature of these responses was confirmed using blocking Clr-b mAb (data not shown), as well as using mutant NIH 3T3.ΔClrb cells infected with each of the MCMV strains (Figures S7B–S7D). Together, these data demonstrate that m12 is a non-redundant NKR-P1B decoy immunoevasin and that the *m12* G271A SNP (E91K polymorphism) identified between MCMV^{Smith} and MCMV^{MW97} is responsible for the differential stimulation of BWZ.P1B reporter cells.

Next, we conducted ^{51}Cr-release cytotoxicity assays using sorted B6-strain NKR-P1B^{+} and NKR-P1B^{-} NK-LAK effectors and MCMV-infected NIH 3T3 targets. Notably, mock, MCMV^{MW97}, and Δm12-infected NIH 3T3 targets were efficiently lysed, whereas m12^{Smith}-infected targets displayed significantly lower cytotoxicity in response to NKR-P1B^{+} effectors (Figure 7D). Importantly, inhibition by m12^{Smith} was NKR-P1B dependent, as it was not observed using NKR-P1B^{-} NK-LAK (Figure 7E). These data reveal that m12^{Smith}, but not m12^{MW97}, is directly capable of inhibiting B6-strain NK cytotoxicity in an NKR-P1B-dependent manner upon live MCMV infection.

To evaluate m12 immunoevasin function in vivo, the three variant MCMV^{MW97} strains were used to infect B6-strain WT, Clr-b$^{-/-}$, and Nkrp1b$^{-/-}$ mice, then MCMV virulence was evaluated 3 days later using plaque assays and quantitative real-time PCR (qPCR) for viral genomic copy numbers in infected spleens. As expected, due to weak interaction between m12^{MW97} and NKR-P1B^{B6}, no significant difference was observed between the parental MCMV^{MW97} and Δm12 mutant viruses in B6 WT mice in vivo (Figure 7F); remarkably, however, the m12^{Smith}-revertant virus displayed significantly higher splenic viral titers (PFU) and viral genomic copy numbers in B6 WT mice (Figures 7F–7G). Importantly, the enhanced virulence of the m12^{Smith} allele in vivo was NKR-P1B dependent and Clr-b independent, as it was not observed using B6-strain Nkrp1b$^{-/-}$ mice (Figures 7F–7G), yet Clr-b$^{-/-}$ mice displayed a similar trend to WT B6 mice (data not shown). Notably, increased virulence of MCMV^{Smith} in vivo has been previously observed using WT B6 mice relative to B6.*Nkrp1b*$^{-/-}$ mice (Rahim et al., 2016). This finding is confirmed to be m12-dependent here using the three MCMV^{MW97}-strain variants, where the m12^{Smith}-revertant virus exhibits enhanced virulence versus parental MCMV^{MW97} and Δm12 mutant MCMV, in WT B6, but not B6.*Nkrp1b*$^{-/-}$, mice. These findings confirm a non-redundant NKR-P1B immunoevasin function for m12 in vivo.

To further elucidate the effects of the polymorphic host NKR-P1A/B/C-clade isoforms and alleles, we next performed in vivo experiments in the FVB, 129, and BALB inbred mouse strains using the three allelic MCMV variants. In the FVB strain, where strong interactions are observed between m12^{Smith} and both the inhibitory NKR-P1B^{FVB} and stimulatory NKR-P1C^{FVB} receptors (Figures 6F–6G), m12^{Smith} function may be counterbalanced by the paired receptors. However, the m12^{MW97} immunoevasin function should be intact, since a moderate interaction is observed for the inhibitory NKR-P1B^{FVB} receptor yet a much weaker interaction for the stimulatory NKR-P1C^{FVB} receptor (Figures 6F–6G). Interestingly, in FVB mice, no significant difference was observed between the m12^{Smith}-revertant and Δm12 mutant viruses in vivo, while the parental MCMV^{MW97} virus maintained significantly elevated viral titers (Figure 7H). Thus, the m12^{MW97} allele possesses superior immunoevasin function in the FVB strain, where the m12^{Smith} allele encounters opposing function from the activating NKR-P1C^{FVB} (and perhaps NKR-P1A^{FVB}) paralog.

(G) Quantitative real-time PCR analysis of MCMV ie1 genomic DNA copy numbers relative to host c-*myc* (*ie1/Myc*); all values from two independent experiments were normalized relative to values from WT B6 mice infected with parental WT virus (m12^{MW97}). Data are pooled from two independent infections using 1x10^{6} or 1x10^{5} PFU/mouse.

(H) Viral PFU titers in spleens of inbred FVB mice infected in vivo using the above MCMV variants and analyzed 3 days post-infection with 5x10^{5} PFU/mouse.

(I–K) Viral splenic titers from (I) BALB/c, 129, (J) B6.*Ly49H*$^{-/-}$, and (K) BALB.B6-Cmv1^{r} mice, respectively, infected in vivo using MCMV variants, analyzed 3 days post-infection with 2x10^{5} PFU/mouse. For (F–K), Mean±SEM are shown, each data point representing an independent mouse, and significance determined by one-way ANOVA (F–J) or unpaired student's t-test (K).

On the other hand, in BALB/c and 129-strain mice, small but significant differences were observed only between the parental MCMV^{MW97} and Δm12 mutant viruses in vivo, with the m12^{Smith}-revertant virus showing an intermediate response (Figure 7I). Interestingly, the published BALB/c and 129-strain NKR-P1A/B/C alleles are identical. In keeping with this, we previously observed moderate interactions between the inhibitory NKR-P1B$^{BALB/129}$ receptor and most m12 alleles (Figure 6D), no interactions between the stimulatory NKR-P1C$^{BALB/129}$ receptor and any m12 alleles (Figure 6E), and a weak interaction for the stimulatory NKR-P1A$^{BALB/129}$ receptor and m12^{Smith} (Figures 2H and 3E); thus, these in vivo results predict that the NKR-P1A$^{BALB/129}$ receptor may have a higher affinity for m12^{MW97} versus m12^{Smith}, in turn resulting in lower viral titers. Notably, while NKR-P1B$^{BALB/129}$ appears to be functional upon overexpression, m12^{Smith} tetramers fail to stain ex vivo NK cells from the BALB/c and 129 strains (Figure S3A), suggesting that both the NKR-P1B/C$^{129/BALB}$ receptors may be non-functional in vivo, in turn resulting in reliance on NKR-P1A$^{129/BALB}$ alone.

To further validate the NKR-P1B-decoy function of the m12 immunoevasin, we also performed in vivo infections using cohorts of B6.*Ly49H*$^{-/-}$ mice, which lack the dominant Ly49H^{B6} activating receptor that recognizes m157, and BALB.B6^{Cmv1r} congenic mice, which are NK1.1^{+} and retain the B6-strain *Nkrp1* genes. Here, the dominant decoy function of the m12^{Smith}-revertant significantly augmented viral PFU titers in both the B6.*Ly49H*$^{-/-}$ (Figure 7J) and BALB.B6^{Cmv1r} (Figure 7K) congenic host strains, relative to the Δm12 mutant and parental m12^{MW97} viruses. These data confirm that the superior decoy function of the m12^{Smith} allele versus the m12^{MW97} allele is enhanced in the absence of Ly49H, segregates with the B6-strain NKR-P1 (*Klrb1*) region, and is unaffected by epistatic effects from the BALB genomic background.

Taken together, the above findings demonstrate that the immunoevasin function of m12 in vivo is both host and virus strain dependent, and it can be functionally counterbalanced by both inhibitory and stimulatory NKR-P1A/B/C-clade polymorphisms and paralogs. These findings further confirm that complex interactions between host NKR and MCMV immunoevasins ultimately determine the outcome of host-pathogen interactions in vivo.

DISCUSSION

The NK1.1 (NKR-P1; *Klrb1*) receptor family comprises both activating and inhibitory members, with a bona fide ligand of the activating NK1.1 antigen remaining unknown, despite being described 40 years ago (Glimcher et al., 1977). We have identified m12 as a natural (viral) ligand for the prototypical NK1.1 antigen, the stimulatory NKR-P1C^{B6} orphan receptor (Glimcher et al., 1977; Koo and Peppard, 1984; Ryan et al., 1992). In addition, host Clr-b represents a second (self) NKR-P1C ligand in the FVB mouse strain. Moreover, we show that m12 functions as a decoy immunoevasin to subvert NK cell-mediated cytotoxicity by direct interaction with the inhibitory NKR-P1B receptor, which normally surveys infected cells for Clr-b downregulation during infection. The identification of the distantly Ig-related m02-family member, m12, as an NKR-P1A/B/C-clade ligand demonstrates sophisticated viral utilization of this protein fold to directly engage an NKR. Structurally, m12 clamped around the NKR-P1B receptor, in a polar claw mechanism, enveloping an extensive area of NKR-P1B that simultaneously provided insight into the specific targeting of the receptor by m12 and how allelic differences in this axis impacted upon recognition. Here, a number of the allelic polymorphisms in both the m12 immunoevasin and NKR-P1 receptors either mapped to the binding site or were in close proximity to it, thereby implying that both direct and indirect effects can impact the m12-NKR-P1 recognition axis.

The m12 footprint overlapped extensively with that observed for binding of the endogenous self ligand, KACL, to the closely related human NKp65 receptor (Li et al., 2013). Indeed, the utilization of existing binding sites on host receptors/ligands appears to be a common viral immune evasion strategy. Nonetheless, such structural mimicry does not necessarily underpin immunoevasin strategies, as structurally diverse immunoevasins, such as HCMV UL16 and MCMV m152, map to the same sites on ligands for the human and mouse activating NKG2D receptors, respectively (Müller et al., 2010; Wang et al., 2012). Further, some viral immunoevasins, including m157, can adopt unusual and unanticipated binding modes (Berry et al., 2013). Our work shows how the structurally divergent, viral Ig-like m12 immunoevasin utilizes binding mode mimicry to engage the inhibitory NKR-P1B receptor, which then underpins the ability of m12 to be reciprocally targeted by the structurally related activating NKR-P1A/C family members, in turn countering the m12 immunoregulatory properties.

The rodent *Klrb1* genes display considerable polymorphism, being subdivided into two antigenic and phylogenetic clusters in mice and rats: the NKR-P1A/B/C and NKR-P1F/G clades (Carlyle et al., 2008; Kirkham and Carlyle, 2014; Kveberg et al., 2009). Strikingly, the NKR-P1B and NKR-P1C receptors appear to have undergone parallel divergence characteristic of paired recognition receptors, leading to the hypothesis that they are under selective pressure, within the constraints imposed by both endogenous self ligands and foreign viral ligands. Here, we provide compelling evidence of co-evolution at the host-pathogen interface, with host adaptation of the NKR-P1A and NKR-P1C (NK1.1) stimulatory receptor paralogs to directly recognize the m12 decoy, as well as the existence of wild-derived viral m12 immunoevasin alleles, including loss-of-function alleles, which may have evolved to avert direct NKR-P1A/C-mediated NK cell activation. We also provide strong evidence that m12 is a non-redundant NKR-P1B-targeting immunoevasin in vivo. However, the functional contribution of m12 to the outcome of host-pathogen interactions in vivo is ultimately determined by both the viral m12 and host NKR-P1A/B/C-clade polymorphisms.

For example, each m12 allele may contribute differentially to viral fitness in distinct mouse strains, and what may appear to be a superior immunoevasin in one mouse strain may be counterbalanced by opposing signals from both inhibitory NKR-P1B and activating NKR-P1A/C paralogs in another mouse strain. Our in-depth analyses employing eight inbred, mutant, or congenic mouse strains and three MCMV variants underscore how viral versus host fitness can be significantly impacted by polymorphisms in both the paired host receptors and viral immunoevasin.

The conserved use of decoy immunoevasins by MCMV (m12) and RCMV (RCTL) to subvert NKR-P1B-mediated NK cell immunosurveillance of pathological target cells highlights the role of the NKR-P1:Clr recognition axis in immunity to infectious disease and suggests that similar mechanisms may operate during HCMV infection of human cells (Aguilar et al., 2015; Voigt et al., 2007). Notably, the human NKR-P1A:LLT1 receptor-ligand pair are likely orthologous to some rodent NKR-P1:Clr interactions. NKR-P1A (CD161) is inhibitory and is expressed on ~60% of human NK cells (Lanier et al., 1994), resembling NKR-P1B in function and expression. LLT1 has more restricted expression than Clr-b and is induced in response to PRR agonists and infection (Aguilar et al., 2015; Germain et al., 2011; Rosen et al., 2008). It remains to be determined whether HCMV may similarly target the human NKR-P1A receptor.

The NK1.1 antigen was the prototypical receptor identified to be selectively expressed by NK cells. Thus, while being used as a tool to study and purify NK cells for almost four decades, the physiological ligand for the activating NK1.1 antigen has remained a mystery. Here, we showcase m12 as a natural virally encoded ligand for this important NKR family. Moreover, NK1.1 is also found on some ILC and various T cell subsets, including invariant NKT cells, the ubiquitous mucosal-associated invariant T (MAIT) cells, $CD4^+$ T helper cells, and activated $CD8^+$ T cells. Thus, targeting of the NK1.1 antigen by a virally encoded ligand has important implications for both innate and adaptive immunity, virus-host co-evolution, and immunotherapy.

STAR★METHODS

Detailed methods are provided in the online version of this paper and include the following:

- KEY RESOURCES TABLE
- CONTACT FOR REAGENTS AND RESOURCES SHARING
- EXPERIMENTAL MODEL AND SUBJECT DETAILS
  - Animals
  - Viruses
  - Cells
- METHOD DETAILS
  - Virus infections
  - Flow cytometry and antibodies
  - BWZ Reporter Cell Assays
  - ^{51}Chromium release cytotoxicity assays
  - Generation of NIH 3T3.ΔClr-b cells using CRISPR-Cas9 technology
  - Protein expression and purification
  - Surface plasmon resonance (SPR)
  - Crystallization and data collection
  - Structure determination and refinement
  - DNA/RNA Isolation, cDNA synthesis and PCR cloning
  - Immunoprecipitations and Western Blotting
  - RNA-Sequencing and Analysis
  - Bioinformatic analysis
- QUANTITATION AND STATISTICAL ANALYSIS
- DATA AND SOFTWARE AVAILABILITY

SUPPLEMENTAL INFORMATION

Supplemental Information includes seven figures and five tables and can be found with this article online at http://dx.doi.org/10.1016/j.cell.2017.03.002.

AUTHOR CONTRIBUTIONS

O.A.A. designed, performed, and analyzed experiments and contributed to the manuscript writing. R.B. and Z.F. generated the purified m12 and NKR-P1 proteins and performed SPR analyses. R.B. solved, refined, and analyzed the structure and contributed to manuscript writing. M.M.A.R., M.T., B.P., M.M.T., and A.B.M. assisted with in vivo experiments. J.J.R. generated the m12 mutant and revertant viruses. T.N.H.L assisted with bioinformatic analysis. G.R.B. assisted with the structural analysis. C.L.K, A.M., B.P., and A.K. assisted with in vitro experiments. D.S.J.A., A.P.M., S.J., J.R., and J.R.C. contributed to the direction of the study. This work was done in the labs of A.P.M., S.J., J.R., and J.R.C. J.R.C. contributed to the design and interpretation of experiments, project management, and manuscript writing.

ACKNOWLEDGMENTS

We would like to thank Drs. S. Vidal, M.G. Brown, K. Iizuka, W. Yokoyama, and T. Mallevaey for reagents and Y. Amemiya, G. Awong, and G. Knowles for services. We also acknowledge the Monash Macromolecular Crystallization Facility and the staff at the Australian Synchrotron. O.A.A. was supported by a Natural Sciences and Engineering Research Council of Canada (NSERC) Post-Graduate Scholarship-Doctoral Award; A.M. by a Canadian Institutes of Health Research (CIHR) Vanier Scholarship; C.L.K. by an Ontario Graduate Scholarship Award. R.B. is a recipient of a National Health and Medical Research Council of Australia (NHMRC) Career Development Award (APP1109901). J.R. is a recipient of an Australian Research Council Laureate Fellowship (FL160100049). A.K. is supported by the Croatian Science Foundation (Grant #7132). S.J. is supported by an Advanced Grant from the European Research Council (ERC #322693). This work was supported by CIHR Operating Grants (#86630 to A.P.M. and J.R.C.; #106491 to J.R.C.), an Early Researcher Award from the Ontario Ministry of Research and Innovation (#RE07-04-071 to J.R.C.), a CIHR New Investigator Award (to J.R.C.), and an Investigator in the Pathogenesis of Infectious Disease Award from the Burroughs Wellcome Fund (#1007761 to J.R.C.).

Received: September 16, 2016
Revised: January 9, 2017
Accepted: February 27, 2017
Published: March 23, 2017

REFERENCES

Aguilar, O.A., Mesci, A., Ma, J., Chen, P., Kirkham, C.L., Hundrieser, J., Voigt, S., Allan, D.S., and Carlyle, J.R. (2015). Modulation of Clr ligand expression and NKR-P1 receptor function during murine cytomegalovirus infection. J. Innate Immun. *7*, 584–600.

Arase, H., Mocarski, E.S., Campbell, A.E., Hill, A.B., and Lanier, L.L. (2002). Direct recognition of cytomegalovirus by activating and inhibitory NK cell receptors. Science *296*, 1323–1326.

Berry, R., Ng, N., Saunders, P.M., Vivian, J.P., Lin, J., Deuss, F.A., Corbett, A.J., Forbes, C.A., Widjaja, J.M., Sullivan, L.C., et al. (2013). Targeting of a natural killer cell receptor family by a viral immunoevasin. Nat. Immunol. *14*, 699–705.

Berry, R., Vivian, J.P., Deuss, F.A., Balaji, G.R., Saunders, P.M., Lin, J., Littler, D.R., Brooks, A.G., and Rossjohn, J. (2014). The structure of the cytomegalovirus-encoded m04 glycoprotein, a prototypical member of the m02 family of immunoevasins. J. Biol. Chem. *289*, 23753–23763.

Carlyle, J.R., Jamieson, A.M., Gasser, S., Clingan, C.S., Arase, H., and Raulet, D.H. (2004). Missing self-recognition of Ocil/Clr-b by inhibitory NKR-P1 natural killer cell receptors. Proc. Natl. Acad. Sci. USA *101*, 3527–3532.

Carlyle, J.R., Martin, A., Mehra, A., Attisano, L., Tsui, F.W., and Zúñiga-Pflücker, J.C. (1999). Mouse NKR-P1B, a novel NK1.1 antigen with inhibitory function. J. Immunol. *162*, 5917–5923.

Carlyle, J.R., Mesci, A., Fine, J.H., Chen, P., Bélanger, S., Tai, L.H., and Makrigiannis, A.P. (2008). Evolution of the Ly49 and Nkrp1 recognition systems. Semin. Immunol. *20*, 321–330.

Carlyle, J.R., Mesci, A., Ljutic, B., Belanger, S., Tai, L.H., Rousselle, E., Troke, A.D., Proteau, M.F., and Makrigiannis, A.P. (2006). Molecular and genetic basis for strain-dependent NK1.1 alloreactivity of mouse NK cells. J. Immunol. *176*, 7511–7524.

Chen, P., Aguilar, O.A., Rahim, M.M., Allan, D.S., Fine, J.H., Kirkham, C.L., Ma, J., Tanaka, M., Tu, M.M., Wight, A., et al. (2015). Genetic investigation of MHC-independent missing-self recognition by mouse NK cells using an in vivo bone marrow transplantation model. J. Immunol. *194*, 2909–2918.

Chen, P., Bélanger, S., Aguilar, O.A., Zhang, Q., St-Laurent, A., Rahim, M.M., Makrigiannis, A.P., and Carlyle, J.R. (2011). Analysis of the mouse 129-strain Nkrp1-Clr gene cluster reveals conservation of genomic organization and functional receptor-ligand interactions despite significant allelic polymorphism. Immunogenetics *63*, 627–640.

Fine, J.H., Chen, P., Mesci, A., Allan, D.S., Gasser, S., Raulet, D.H., and Carlyle, J.R. (2010). Chemotherapy-induced genotoxic stress promotes sensitivity to natural killer cell cytotoxicity by enabling missing-self recognition. Cancer Res. *70*, 7102–7113.

Fodil-Cornu, N., Lee, S.H., Belanger, S., Makrigiannis, A.P., Biron, C.A., Buller, R.M., and Vidal, S.M. (2008). Ly49h-deficient C57BL/6 mice: a new mouse cytomegalovirus-susceptible model remains resistant to unrelated pathogens controlled by the NK gene complex. J. Immunol. *181*, 6394–6405.

Germain, C., Meier, A., Jensen, T., Knapnougel, P., Poupon, G., Lazzari, A., Neisig, A., Håkansson, K., Dong, T., Wagtmann, N., et al. (2011). Induction of lectin-like transcript 1 (LLT1) protein cell surface expression by pathogens and interferon-γ contributes to modulate immune responses. J. Biol. Chem. *286*, 37964–37975.

Glimcher, L., Shen, F.W., and Cantor, H. (1977). Identification of a cell-surface antigen selectively expressed on the natural killer cell. J. Exp. Med. *145*, 1–9.

Iizuka, K., Naidenko, O.V., Plougastel, B.F., Fremont, D.H., and Yokoyama, W.M. (2003). Genetically linked C-type lectin-related ligands for the NKRP1 family of natural killer cell receptors. Nat. Immunol. *4*, 801–807.

Kirkham, C.L., and Carlyle, J.R. (2014). Complexity and Diversity of the NKR-P1:Clr (Klrb1:Clec2) Recognition Systems. Front. Immunol. *5*, 214.

Kolenko, P., Rozbeský, D., Vaněk, O., Kopecký, V., Jr., Hofbauerová, K., Novák, P., Pompach, P., Hašek, J., Skálová, T., Bezouška, K., and Dohnálek, J. (2011). Molecular architecture of mouse activating NKR-P1 receptors. J. Struct. Biol. *175*, 434–441.

Koo, G.C., and Peppard, J.R. (1984). Establishment of monoclonal anti-Nk-1.1 antibody. Hybridoma *3*, 301–303.

Kveberg, L., Dai, K.Z., Westgaard, I.H., Daws, M.R., Fossum, S., Naper, C., and Vaage, J.T. (2009). Two major groups of rat NKR-P1 receptors can be distinguished based on chromosomal localization, phylogenetic analysis and Clr ligand binding. Eur. J. Immunol. *39*, 541–551.

Lanier, L.L., Chang, C., and Phillips, J.H. (1994). Human NKR-P1A. A disulfide-linked homodimer of the C-type lectin superfamily expressed by a subset of NK and T lymphocytes. J. Immunol. *153*, 2417–2428.

Li, Y., Wang, Q., Chen, S., Brown, P.H., and Mariuzza, R.A. (2013). Structure of NKp65 bound to its keratinocyte ligand reveals basis for genetically linked recognition in natural killer gene complex. Proc. Natl. Acad. Sci. USA *110*, 11505–11510.

Mesci, A., and Carlyle, J.R. (2007). A rapid and efficient method for the generation and screening of monoclonal antibodies specific for cell surface antigens. J. Immunol. Methods *323*, 78–87.

Müller, S., Zocher, G., Steinle, A., and Stehle, T. (2010). Structure of the HCMV UL16-MICB complex elucidates select binding of a viral immunoevasin to diverse NKG2D ligands. PLoS Pathog. *6*, e1000723.

Rahim, M.M., Chen, P., Mottashed, A.N., Mahmoud, A.B., Thomas, M.J., Zhu, Q., Brooks, C.G., Kartsogiannis, V., Gillespie, M.T., Carlyle, J.R., and Makrigiannis, A.P. (2015). The mouse NKR-P1B:Clr-b recognition system is a negative regulator of innate immune responses. Blood *125*, 2217–2227.

Rahim, M.M., Wight, A., Mahmoud, A.B., Aguilar, O.A., Lee, S.H., Vidal, S.M., Carlyle, J.R., and Makrigiannis, A.P. (2016). Expansion and protection by a virus-specific NK cell subset lacking expression of the inhibitory NKR-P1B receptor during murine cytomegalovirus infection. J. Immunol. *197*, 2325–2337.

Raulet, D.H., and Vance, R.E. (2006). Self-tolerance of natural killer cells. Nat. Rev. Immunol. *6*, 520–531.

Rosen, D.B., Cao, W., Avery, D.T., Tangye, S.G., Liu, Y.J., Houchins, J.P., and Lanier, L.L. (2008). Functional consequences of interactions between human NKR-P1A and its ligand LLT1 expressed on activated dendritic cells and B cells. J. Immunol. *180*, 6508–6517.

Ryan, J.C., Turck, J., Niemi, E.C., Yokoyama, W.M., and Seaman, W.E. (1992). Molecular cloning of the NK1.1 antigen, a member of the NKR-P1 family of natural killer cell activation molecules. J. Immunol. *149*, 1631–1635.

Scalzo, A.A., Lyons, P.A., Fitzgerald, N.A., Forbes, C.A., and Shellam, G.R. (1995). The BALB.B6-Cmv1r mouse: a strain congenic for Cmv1 and the NK gene complex. Immunogenetics *41*, 148–151.

Sgourakis, N.G., Natarajan, K., Ying, J., Vogeli, B., Boyd, L.F., Margulies, D.H., and Bax, A. (2014). The structure of mouse cytomegalovirus m04 protein obtained from sparse NMR data reveals a conserved fold of the m02-m06 viral immune modulator family. Structure *22*, 1263–1273.

Smith, L.M., McWhorter, A.R., Shellam, G.R., and Redwood, A.J. (2013). The genome of murine cytomegalovirus is shaped by purifying selection and extensive recombination. Virology *435*, 258–268.

Voigt, S., Mesci, A., Ettinger, J., Fine, J.H., Chen, P., Chou, W., and Carlyle, J.R. (2007). Cytomegalovirus evasion of innate immunity by subversion of the NKR-P1B:Clr-b missing-self axis. Immunity *26*, 617–627.

Wagner, M., and Koszinowski, U.H. (2004). Mutagenesis of viral BACs with linear PCR fragments (ET recombination). Methods Mol. Biol. *256*, 257–268.

Wang, R., Natarajan, K., Revilleza, M.J., Boyd, L.F., Zhi, L., Zhao, H., Robinson, H., and Margulies, D.H. (2012). Structural basis of mouse cytomegalovirus m152/gp40 interaction with RAE1γ reveals a paradigm for MHC/MHC interaction in immune evasion. Proc. Natl. Acad. Sci. USA *109*, E3578–E3587.

Williams, K.J., Wilson, E., Davidson, C.L., Aguilar, O.A., Fu, L., Carlyle, J.R., and Burshtyn, D.N. (2012). Poxvirus infection-associated downregulation of C-type lectin-related-b prevents NK cell inhibition by NK receptor protein-1B. J. Immunol. *188*, 4980–4991.

STAR★METHODS

KEY RESOURCES TABLE

REAGENT or RESOURCE	SOURCE	IDENTIFIER
Antibodies		
Rat anti-mouse Clr-b monoclonal (clone 4A6)	Carlyle et al., 2004	N/A
Anti-NKR-P1B antibody monoclonal (clone 2D12)	Iizuka et al., 2003	N/A
Anti-NKR-P1C/NK1.1 monoclonal (clone PK136)	eBioscience	Cat# 13-5941-85; RRID: AB_466805
Anti-NKp46 monoclonal, FITC conjugated (clone 29A1.4)	eBioscience	Cat# 11-3351-82; RRID: AB_1210843
Anti-CD3ε monoclonal, APC-conjugated (clone 145-2C11)	eBioscience	Cat# 17-0031-83; RRID: AB_469316
Anti-FLAG epitope monoclonal (clone M2)	Sigma-Aldrich	Cat# F9291; RRID: AB_439698
Anti- FcγRII/III monoclonal (clone 2.4G2)	eBioscience	Cat# 14-0161-86; RRID: AB_467135
Anti-CD49b monoclonal, PE-Cy7 conjugated (clone DX5)	eBioscience	Cat# 25-5971-82; RRID: AB_469667
Anti-γδTCR monoclonal, PE-Cy7 conjugated (clone GL3)	eBioscience	Cat# 25-5711-80, also 25-5711; RRID: AB_2573463
CD1d–tetramer loaded with PBS-57, an analog of αGalactosylCeramide	NIH	N/A
Streptavidin conjugated APC	Thermo Fisher Scientific	Cat# S868
Streptavidin conjugated PE	Thermo Fisher Scientific	Cat# S866
MCMV $m12^{Smith}$-tetramer	This paper	N/A
NKR-$P1B^{B6}$-tetramer	This paper	N/A
NKR-$P1B^{129}$-tetramer	This paper	N/A
NKR-$P1B^{FVB}$-tetramer	This paper	N/A
Anti-mouse NK1.1 (CD161) (for SPR)	StemCell Technologies, Inc.	Cat# 60103
Chemicals, Peptides, and Recombinant Proteins		
MCMV $m12^{Smith}$	This paper	N/A
NKR-$P1B^{129}$	This paper	N/A
NKR-$P1B^{129}$	This paper	N/A
NKR-$P1B^{FVB}$	This paper	N/A
NKR-$P1C^{B6}$	This paper	N/A
MCMV $m04^{Smith}$	Berry et al., 2014	N/A
$Ly49A^{B6}$	Berry et al., 2013	N/A
Recombinant human IL-2 (Proleukin)	Novartis	Proleukin (aldesleukin)
Radioactive Sodium chromate ($Na_2{}^{51}CrO_4$)	Perkin-Elmer	Cat# NEZ030S001MC
chlorophenol-red-β-D-galactopyranoside, CPRG	Roche Diagnostics	Cat# 10884308001
$Lipofectamine^{2000}$	Thermo Fisher Scientific	Cat# 11668019
D-biotin	Sigma-Aldrich	Cat# 47868
PEG400	Sigma-Aldrich	Cat# 202398
Bis/Tris	Sigma-Aldrich	Cat# B9754
Cellfectin2	Invitrogen	Cat# 10362100
Insect-XPRESS medium	Lonza	Cat# 12-730Q
P20	GE Healthcare	Cat# BR100054
Critical Commercial Assays		
Streptavidin coated chips	GE Healthcare	Cat# BR100032
HisTrap columns	GE Healthcare	Cat# 17-5248-02
Superdex200 16/60 column	GE Healthcare	Cat# 28989335
Total RNA Purification Plus Kit	Norgen Biotek	Cat# 48400

(*Continued on next page*)

Continued

REAGENT or RESOURCE	SOURCE	IDENTIFIER
miRVana miRNA Isolation kit	Thermo Fisher Scientific	Cat# AM1560
Q5 High-Fidelity DNA Polymerase Mix	New England Biolabs	Cat# M0492S
Easy-DNA gDNA Purification Kit	Thermo Fisher Scientific	K180001
Deposited Data		
Co-crystal structure of NKR-P1B^{B6} and m12^{Smith}	This paper	PDB: 5TZN
FVB-strain sequences, Nkrp1 splice variants, and MCMV m12 sequences	This paper	GenBank: KX443605–KX443630
Murid Herpesvirus 1 strain Smith, complete genome	https://www.ncbi.nlm.nih.gov/nuccore/GU305914	GenBank: GU305914.1
Experimental Models: Cell Lines		
Mouse: NIH 3T3	ATCC	Cat# CRL-1658; RRID: CVCL_0594
Mouse: NIH 3T3.ΔClrb	This paper	N/A
Mouse: BWZ.36	Mesci and Carlyle, 2007	N/A
Mouse: YAC-1	ATCC	Cat# TIB-160; RRID: CVCL_2244
Mouse: embryonic fibroblasts	Laboratory of Tak Mak	N/A
Human: HEK293T	Laboratory of David Raulet	N/A
Human: HEK293S GnTi-	ATCC (In vitro Technologies)	Cat# CRL-3022; RRID: CVCL_A785
Hi5 insect cells	Life Technologies	Cat# B855-02
Sf9 insect cells	Thermo Fischer Scientific	Cat# 11496-015
DH10Bac *E.coli* cells	Thermo Fischer Scientific	Cat# 10361-012
OneShot TOP10 chemically competent *E.coli* cells	Thermo Fisher Scientific	Cat# C404003
Experimental Models: Organisms/Strains		
Mouse: C57BL/6	Jackson Laboratories	RRID: IMSR_JAX:000664
Mouse: FVB/N	Taconic	Cat# FVB
Mouse: 129S6	Taconic	Cat# 129SVE
Mouse: BALB/c	Taconic	Cat# BALB
Mouse: B6.Clrb$^{-/-}$	Chen et al., 2015	N/A
Mouse: B6.Nkrp1b$^{-/-}$	Rahim et al., 2015	N/A
Mouse: B6.Ly49h$^{-/-}$	Fodil-Cornu et al., 2008	N/A
Mouse: Balb.B6-Cmv1^{r}	Scalzo et al., 1995	N/A
MCMV: Smith	Laboratory of Silvia Vidal	N/A
MCMV: MCMV-GFP (Smith strain)	Laboratory of Silvia Vidal	N/A
MCMV: K181	Laboratory of Michael Brown	N/A
MCMV: MW97.01 (BAC-generated)	Laboratory of Stipan Jonjic	N/A
MCMV: MW97.01.Δm12	This paper	N/A
MCMV: MW97.01.m12^{Smith}	This paper	N/A
Recombinant DNA		
pIRES2-EGFP	Clontech	N/A – discontinued vector
pMSCV2.2-IRES-EGFP	Carlyle et al., 2004	N/A
pMSCV2.2-IRES-EGFP Type I CD3ζ fusion vector	Mesci and Carlyle, 2007	N/A
pMSCV2.2-IRES-EGFP Type II CD3ζ fusion vector	Mesci and Carlyle, 2007	N/A
pSpCas9(BB)-2A-GFP (PX458)		Addgene plasmid #48138
pSm3fr BAC (MW97.01 BAC)	Wagner and Koszinowski, 2004	N/A
pFastbac	Thermo Fisher Scientific	Cat# 10712-024

(*Continued on next page*)

Continued

REAGENT or RESOURCE	SOURCE	IDENTIFIER
pHLSec	Laboratory of Radu Aricescu	N/A
Synthetic genes for NKR-P1B^{B6,129,FVB}, NKR-P1C^{B6} and m12^{Smith}	IDT	N/A
Sequence-Based Reagents		
CMV-for sequencing primer for sequencing pIRES2: 5′- CGCAAATGGGCGGTAGGCGTG-3′	TCAG Facility	N/A
pIRES2 reverse sequencing primer: 5′- AGACCCCTAGGAATGCTCGT-3′	This paper	N/A
MSCV forward sequencing primer (T7 promoter primer): 5′- TAATACGACTCACTATAGGG-3′	TCAG Facility	N/A
MSCV reverse sequencing primer: 5′- GCGGCTTCGGCCAGTAACGTT-3′	Mesci and Carlyle, 2007	N/A
LKO1_5 sequencing primer: 5′- GACTATCATATGCTTACCGT-3′		N/A
Seqm12for forward sequencing primer for m12 BAC mutants: 5′- TCGATAGACACCACGACCCT-3′	This paper	N/A
Seqm12rev reverse sequencing primer for m12 BAC mutants: 5′- CGCCGTTGACTTCGACAAAG-3′	This paper	N/A
Primers for generating constructs, see Table S5	This paper	N/A
Software and Algorithms		
TopHat2	http://ccb.jhu.edu/software/tophat/index.shtml	RRID: SCR_013035
FlowJo	https://www.flowjo.com	RRID: SCR_008520
Bowtie2	http://bowtie-bio.sourceforge.net/bowtie2/index.shtml	RRID: SCR_005476
Integrative Genomics Viewer (IGV version 2.3.34)	https://www.broadinstitute.org/igv/	RRID: SCR_011793
Cufflinks	http://cole-trapnell-lab.github.io/cufflinks/	RRID: SCR_014597
DNASTAR: Lasergene Core Suite (version 8)	https://www.dnastar.com/t-dnastar-lasergene.aspx	RRID: SCR_000291
SignalP4.1 Server	http://www.cbs.dtu.dk/services/SignalP/)	N/A
TMpred	http://www.ch.embnet.org/software/TMPRED_form.html	N/A
NetStart 1.0 Prediction Server	http://www.cbs.dtu.dk/services/NetStart/	N/A
iMosflm	http://www.mrc-lmb.cam.ac.uk/harry/imosflm/ver721/introduction.html	RRID: SCR_014217
Collaborative Computational Project No.4 (CCP4)	http://www.ccp4.ac.uk/	RRID: SCR_007255
BUSTER	https://www.globalphasing.com/buster/	N/A
GraphPad Prism (Version 7)	https://www.graphpad.com/scientific-software/prism/	RRID: SCR_002798
Coot	http://www2.mrc-lmb.cam.ac.uk/personal/pemsley/coot/	RRID: SCR_014222
PyMOL	http://www.pymol.org	RRID: SCR_000305
Adaptive Poisson-Boltzmann Solver (APBS)	http://www.poissonboltzmann.org	RRID: SCR_008387
SCALA	http://www.ccp4.ac.uk/html/scala.html	N/A

CONTACT FOR REAGENTS AND RESOURCES SHARING

As Lead Contact, James R. Carlyle is responsible for all reagent and resource requests. Please contact James Carlyle at james.carlyle@utoronto.ca with requests and inquiries.

EXPERIMENTAL MODEL AND SUBJECT DETAILS

Animals

C57BL/6 (B6) mice were purchase from the Jackson Laboratory, FVB/N (FVB) and 129S6 (129) mice were purchased from Charles River. We have previously described the B6.Nkrp1b$^{-/-}$ and B6.Clrb$^{-/-}$ mice (Chen et al., 2015; Rahim et al., 2015). B6.Ly49h$^{-/-}$ and Balb.B6-Cmv1^{r} mice have previously been described (Fodil-Cornu et al., 2008; Scalzo et al., 1995). All animals were maintained according to approved protocols at the respective institutes: Sunnybrook Research Institute, University of Ottawa, and the University of Rijeka.

Viruses

MCMV (Smith strain), MCMV-GFP, and MW97.01 (BAC-generated strain) have all been previously described (Aguilar et al., 2015). MCMV^{Smith} and MCMV-GFP were provided by Dr. Silvia Vidal (McGill University). The MCMV^{K181} strain was provided by Dr. Michael G. Brown (University of Virginia). The Δm12 mutant virus and m12^{Smith}-revertant viruses were constructed using BAC technology that has previously been described (Wagner and Koszinowski, 2004).

Cells

NIH 3T3, YAC-1, and HEK293T cells were purchased from the American Type and Culture Collection (ATCC). BWZ.36 cells were obtained from N. Shastri (UC Berkeley, CA, USA). B6 mouse embryonic fibroblasts (MEF) were obtained from T.W. Mak (University of Toronto, Canada). Cells were cultured in complete DMEM-HG, supplemented with 2 mM glutamine, 100 U/mL penicillin, 100 μg/ml streptomycin, 50 μg/mL gentamicin, 110 μg/mL sodium pyruvate, 50 μM 2-mercaptoethanol, 10 mM HEPES, and 10% FCS. Cells were maintained in incubator at 37°C, 5% CO_2.

Sf9 and Hi5 cells were cultured in Insect-XPRESS medium (Lonza) at 27°C and maintained with shaking at 120 rpm. HEK293S GnTi- adherent cells were cultured in DMEM supplemented with 10% FBS and 1% Pen/Strep/Glutamine (GIBCO) at 37°C in the presence of 5% CO2. For protein expression, FBS was reduced to 2%.

METHOD DETAILS

Virus infections

All viruses were passaged using MEF cells, and purified according to described protocols (Aguilar et al., 2015). For in vitro infections, mouse fibroblasts were infected with MCMV at an MOI of 0.5 PFU/cell, centrifuged at 800x*g* for 30 min, and incubated at 37°C. For in vivo infections, mice were infected intraperitoneally with 0.2-1x10^{6} PFU and sacrificed on day 3, tissues harvested, and the viral titers were assessed using plaque-forming assays (Aguilar et al., 2015).

Flow cytometry and antibodies

Flow cytometry was performed as previously described (Chen et al., 2015). Clr-b mAb (4A6) has previously been described (Carlyle et al., 2004). The NKR-P1B^{B6} mAb and hybridoma (2D12) were a kind gift from Drs. Koho Izuka and Wayne Yokoyama (Iizuka et al., 2003). All other mAb clones were purchased from eBioscience or Sigma-Aldrich and are has follows: NK1.1 (PK136); NKp46 (29A1.4); CD3ε (145-C11); FcγRII/III (2.4G2); CD49b/DX5 (clone DX5); γδTCR (clone GL3); FLAG (M2); streptavidin, SA-PE/APC (Thermo Fisher Scientific). The CD1d-tetramer loaded with PBS-57 (αGalCer analog) was a kind gift from Dr. Thierry Mallevaey. For tetramerization, purified biotinylated monomers (m12^{Smith}, NKR-P1B^{B6,129,FVB}) were incubated with SA-PE in a 4:1 molar ratio, aliquoted in 1/10th volumes over a 3 hr period at 4°C.

Cells were stained in flow buffer (HBSS, 0.5% BSA and 0.03% NaN_3) on ice with primary monoclonal antibodies for 25-30 min, or secondary streptavidin conjugates for 15-20 min, washed between incubations and then analyzed using a FACSCalibur or FACSCanto II flow cytometer, or FACS sorted using a FACSAria (BD Biosciences). For staining of ex vivo splenocytes or NKp46^{+}CD3^{-} lymphokine-activated killer (NK-LAK) effectors, cells were pre-incubated with 2.4G2 mAb for 10 min on ice prior to staining with antibodies. Cells were stained with tetramers by incubating on ice for 1 hr. Cells were analyzed by live gating for FSC/SSC, doublet excluded, exclusion of propidium iodide or DAPI for viability, and then according to cell surface markers. Flow cytometry files were analyzed using FlowJo software.

BWZ Reporter Cell Assays

The ectodomains of the mouse NKR-P1 genes were PCR amplified from day 6 LAK cDNA (see Table S5 for primers) and cloned into a type-II MSCV vector to make chimeric receptors with intracellular CD3ζ domains. MCMV m12/CD3ζ chimeric reporters were constructed by cloning the ectodomain of m12 into a type-I MSCV vector (Mesci and Carlyle, 2007). Retroviruses produced with these constructs were used to transduce BWZ.36 cells, and then sorted for IRES-GFP^{+} expression. All reporters were sorted to have

matched GFP expression. Reporter assays were done by co-culturing reporter cells ($5x10^4$) with serially diluted amounts of stimulators in 96-well plates. Stimulators used were either MCMV-infected, mock-infected, or cells transfected with plasmids using Lipofectamine^{2000} (Thermo Fisher Scientific). Positive control cells were stimulated with 10 ng/mL PMA plus 0.5 μM ionomycin. These cells were incubated overnight, washed with PBS, then resuspended in 150 μL of 1X CPRG buffer (90 mg/L chlorophenol-red-β-D-galactopyranoside (Roche), 9 mM MgCl2, 0.1% NP-40, in PBS), incubated at room temperature, then analyzed using a Varioskan microplate reader (Thermo Fisher Scientific), using OD 595-655.

^{51}Chromium release cytotoxicity assays

Splenic lymphokine-activated killer (LAK) effector cells were generated by harvesting spleens from mice, processing into single cell suspensions, ACK lysed (Thermo Fisher Scientific), then grown in 10% complete RPMI 1640 media supplemented with 2500 U/mL human rIL-2 (Proleukin; Novartis). On day 4, these cells were FACS sorted for NKp46$^+$CD3$^-$ NK cells subsetted based upon NKR-P1B$^{B6/FVB}$ (2D12 or NK1.1 mAb) expression, and used as effectors in ^{51}Cr-release assays on day 6 or 7. Target cells were labeled with 50 μCi $Na_2{}^{51}CrO_4$ (Perkin Elmer) in FCS for 1 hr at 37°C, washed, plated in 96-well V-bottom plates in serial dilutions with effector cells at corresponding ratios, and incubated at 37°C for 4 hr. Supernatants (100 μl) were then transferred to scintillation plates (LumaPlate-96; Perkin Elmer), dried overnight, and counted using a Top Count NXT microplate Scintillation Counter (Packard Instrument Company). Percent specific lysis values were calculated relative to standard maximum release (2% Triton X-100) and spontaneous release (media) values.

Generation of NIH 3T3.ΔClr-b cells using CRISPR-Cas9 technology

The pX458 vector was utilized in accordance with Dr. Zhang's protocol for generating targeting vectors (www.genome-engineering.org/crispr/). The sequence of oligos used for constructing *Clec2d* targeting vector were: sense: 5′-cac cgC TAC CTA TGC TTA GTC CCA C-3′; anti-sense: 5′-aaa cGT GGG ACT AAG CAT AGG TAG c-3′. This vector was transfected into NIH 3T3 cells that were then sorted for GFP$^+$Clr-b$^-$ expression. These cells were then subcloned using limiting dilution. Appropriate clones were selected lacking Clr-b cell surface staining and BWZ.NKR-P1B reporter stimulation.

Protein expression and purification

Codon optimized genes encoding NKR-P1 receptors and m12 were synthesized by Integrated DNA Technologies. For NKR-P1B^{B6}, the unpaired cysteine residue at position 118 was replaced with a glycine. The ectodomains (residues 89-215) of NKR-P1B^{B6,129,FVB} and NKR-P1C^{B6} were cloned into a modified pHLSec vector upstream of a biotinylation site and a His tag (for SPR) or a His tag (for crystallization), and expressed via transient transfection in HEK293S cells as described previously (Berry et al., 2013; Berry et al., 2014). For a single 6000 cm^3 roller bottle, 600 μg plasmid DNA was mixed with 900 μL PEI (1 mg/ml) and 50 mL serum-free DMEM media. This mixture was added to HEK293S GnTi- cells after a 10 min incubation, followed by the subsequent addition of a further 200 mL DMEM and FCS to give a final concentration of 2%. Media was harvested after 3 and 6 days. DNA encoding m12^{Smith} (residues 29-208) was ligated into the pFastbac vector (ThermoFisher Scientific) upstream of a 6x Histidine tag and used to generate recombinant baculovirus according to the manufacturer's instructions. Specifically, the plasmid was transformed into DH10Bac *E.coli* cells in order to produce bacmid DNA. Recombinant baculoviruses were generated by transfection of Sf9 cells using Cellfectin 2. Protein was expressed in Hi5 insect cells by the addition of 2% P3 virus, and harvested after 48-72h. Cell culture media containing secreted m12 or NKR-P1 receptors was concentrated by tangential flow filtration and purified using nickel affinity and size exclusion chromatography using HisTrap and Superdex 200 columns 16/60 (GE Healthcare) respectively. For biotinylation, purified NKR-P1 receptors were buffer exchanged into 10 mM Tris and biotinylated overnight at 20°C prior to removal of free biotin via size exclusion chromatography. For SPR experiments, m12 protein was used immediately following purification. However, samples stored at 4°C at high concentration were prone to proteolytic degradation, resulting in a loss of ~4 kDa of mass from the carboxy-terminus, as judged by SDS-PAGE analysis. This truncated form of m12 could be selectively purified from the intact molecule by nickel affinity chromatography and bound to NKR-P1 receptors with the same affinity as the entire m12 ectodomain (data not shown). Accordingly, this truncated form of m12 was used for crystallization experiments. The ectodomains of Ly49A^{B6} and m04^{Smith} were produced in HEK293SGnTi- cells as described for NKR-P1 above and previously (Berry et al., 2013; Berry et al., 2014).

Surface plasmon resonance (SPR)

SPR experiments were performed at 25°C on a Biacore 3000 using a running buffer consisting of 10 mM Tris pH8 containing 150 mM NaCl and 0.005% P20. Approximately 800 response units of biotinylated NKR-P1/Ly49 receptors were coupled on to streptavidin-coated chips according to the manufacturer's instructions (GE Healthcare). Remaining free streptavidin sites were blocked with D-biotin. m12 (0.025-50 μM) or m04 (100 μM) was injected over the immobilized receptors at a flow rate of 20 μl/min and the final response was calculated by subtraction of the response of an 'empty' flow cell (containing biotin blocked streptavidin). For blocking experiments, 50 μM m12^{Smith} was passed over immobilized NKR-P1B^{B6} and NKR-P1C^{B6} both before and after injection of 30 μL of 10 μg/ml NK1.1 (clone PK136-StemCell Technologies, Inc.). Equilibrium data were analyzed in GraphPad Prism.

Crystallization and data collection

For crystallization, the m12^{Smith} and NKR-P1B^{B6} ectodomains were mixed in a 1:1 molar ratio at a final protein concentration of 6.5 mg/ml. Crystals were obtained by the hanging drop vapor-diffusion method from a solution containing 41% PEG 400, 0.1 M Bis/Tris pH 6.3 and 0.4 M sodium iodide at 20°C. Crystals were flash cooled using liquid nitrogen and X-ray diffraction data were recorded on a Quantum-315 CCD detector at the MX2 beamline of the Australian Synchrotron. Data were integrated using iMOSFLM and scaled using SCALA from the CCP4 program suite. Details of the data processing statistics are given in Table S3.

Structure determination and refinement

The structure was solved by molecular replacement using the Phaser program. The initial search model comprised a truncated form of the NKR-P1A CTLD (PDB ID: 3M9Z) that lacked the extended loop located between the β3 and β4 strands. The resulting unbiased electron density was not sufficient to build m12 de novo. However, molecular replacement using an extensively truncated fragment of m04 (PDB ID: 4PN6) comprising only the I, D, E' and F strands improved the quality of the electron density map to an extent that allowed the remainder of the m12 molecule to be built. The structure was refined using Buster. Model building was performed in Coot, and figures were prepared with Pymol (http://www.pymol.org) and APBS. Details of the refinement statistics are provided in Table S4.

DNA/RNA Isolation, cDNA synthesis and PCR cloning

Genomic DNA was isolated using Easy-DNA kit (Thermo Fisher Scientific). RNA was isolated using Total RNA isolation kit with gDNA removal (Norgen Biotek) and reverse transcription reactions were done using Superscript III cDNA synthesis kit (Thermo Fisher Scientific). Quantitative RT-PCR was performed on a CFX-96 PCR Detection System (Bio-Rad) using 20-50 ng of cDNA, and PerfeCTa qPCR mix (Quanta Biosciences). The primers used can be found in Table S5.

PCR cloning of m02 and m145 family members was done using gene-specific primers with appropriate restriction enzyme sites, cDNA from MCMV-GFP infected NIH 3T3, amplified with Q5 high-fidelity PCR system (New England Biolabs), and cloned into the pIRES2-EGFP vector (Clontech). The summary of primers can be found in Table S5. The m12^{C4A} gene was synthesized by conducting in situ mutagenesis using primers found in Table S5. The m12^{G4} gene was synthesized using GeneArt services from Thermo Fisher Scientific (Burlington, ON). Cloning of the Nkrp1 genes was mediated by PCR using gene specific primers (Table S5).

Immunoprecipitations and Western Blotting

N-terminally FLAG-tagged constructs of m12 were generated using primers in (Table S5) and cloned into pIRES2-EGFP vector. These constructs were transfected into either HEK293T or NIH 3T3 cells and immunoprecipitations were done using anti-FLAG mAb bound to Protein A/G agarose beads in 1% NP-40 buffer. The isolates were run on SDS-PAGE and transferred to Immobilon PVDF membrane (EMD Millipore) and blotted for anti-FLAG-HRP conjugated antibody (Cell Signal Technologies) and developed with Immobilon ECL reagent. Blots were imaged using a MicroChemi 4.2.

RNA-Sequencing and Analysis

Total RNA from either mock-infected, MCMV-GFP, or MW97.01-infected NIH 3T3 cells using mirVana kit (Thermo Fisher Scientific). These samples were quality checked using an Agilent Bioanalyzer 2100 and confirmed to have RNA integrity values of > 9, then used to create a cDNA library for SOLiD RNA-Sequencing. For analysis of viral transcripts, raw data was mapped onto the MCMV^{Smith} reference genome (accession number GU305914) using TopHat algorithm and Cufflinks was applied to report RPKM values. Mapped reads were visualized using the Integrative Genomics Viewer (IGV version 2.3.34, Broad Institute, https://www.broadinstitute.org/igv/).

Bioinformatic analysis

Mapped RNA-Seq reads were loaded visualized on the IGV Genome Browser using the MCMV^{Smith} reference genome (accession number GU305914). Membrane topology was determined using the TMpred server (http://www.ch.embnet.org/software/TMPRED_form.html). The SignalP 4.1 Server (http://www.cbs.dtu.dk/services/SignalP/) was used for identification of predicted signal peptides. Detection of ORF start site was achieved using the NetStart 1.0 Prediction Server website (http://www.cbs.dtu.dk/services/NetStart/).

QUANTITATION AND STATISTICAL ANALYSIS

Data were analyzed using GraphPad Prism 7, using either a paired Student's two-tailed t test, or one-way/two-way ANOVA, where applicable. See figure legends for details. Statistical significance is defined as: * $p < 0.05$; ** $p < 0.01$; *** $p < 0.001$.

DATA AND SOFTWARE AVAILABILITY

Coordinates for the m12:NKR-P1B structure have been deposited in the protein data bank (PDB: 5TZN). The accession numbers for the FVB-strain sequences, Nkrp1 splice variants, and m12 variants reported in this paper are GenBank: KX443605–GenBank: KX443630.

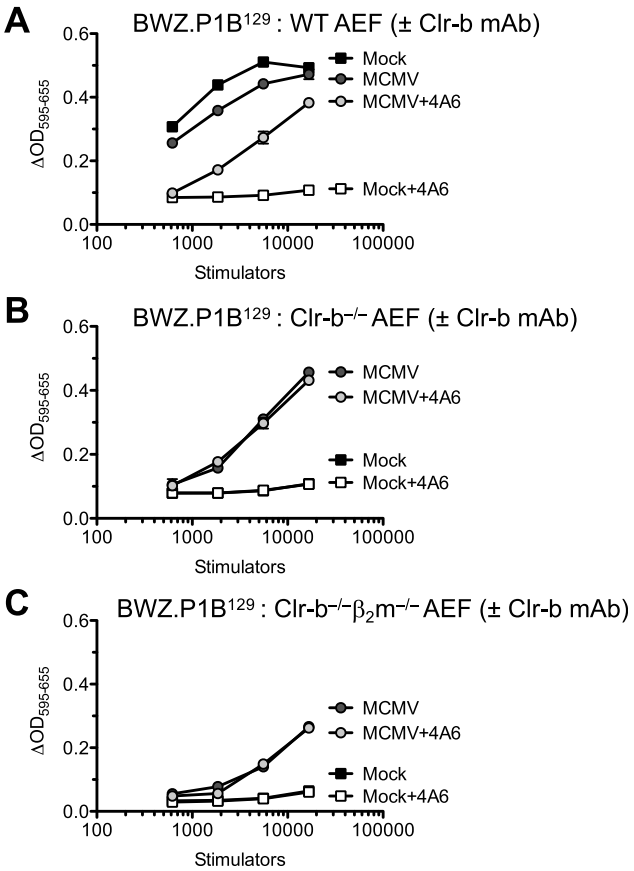

Figure S1. MCMV Encodes a Clr-b and β_2m-Independent NKR-P1B Decoy Ligand, Related to Figure 1

(A–C) Adult ear fibroblasts (AEF) from (A) WT B6, (B) B6.*Clr-b*$^{-/-}$, and (C) B6.*Clr-b*$^{-/-}\beta_2$m$^{-/-}$ mice were infected with MCMV^{Smith} and used as stimulators for BWZ.NKR-P1B^{129} reporter cells in the absence or presence of blocking Clr-b mAb. Mean±SEM are shown in (A) and (B). Data representative of at least 2 independent experiments.

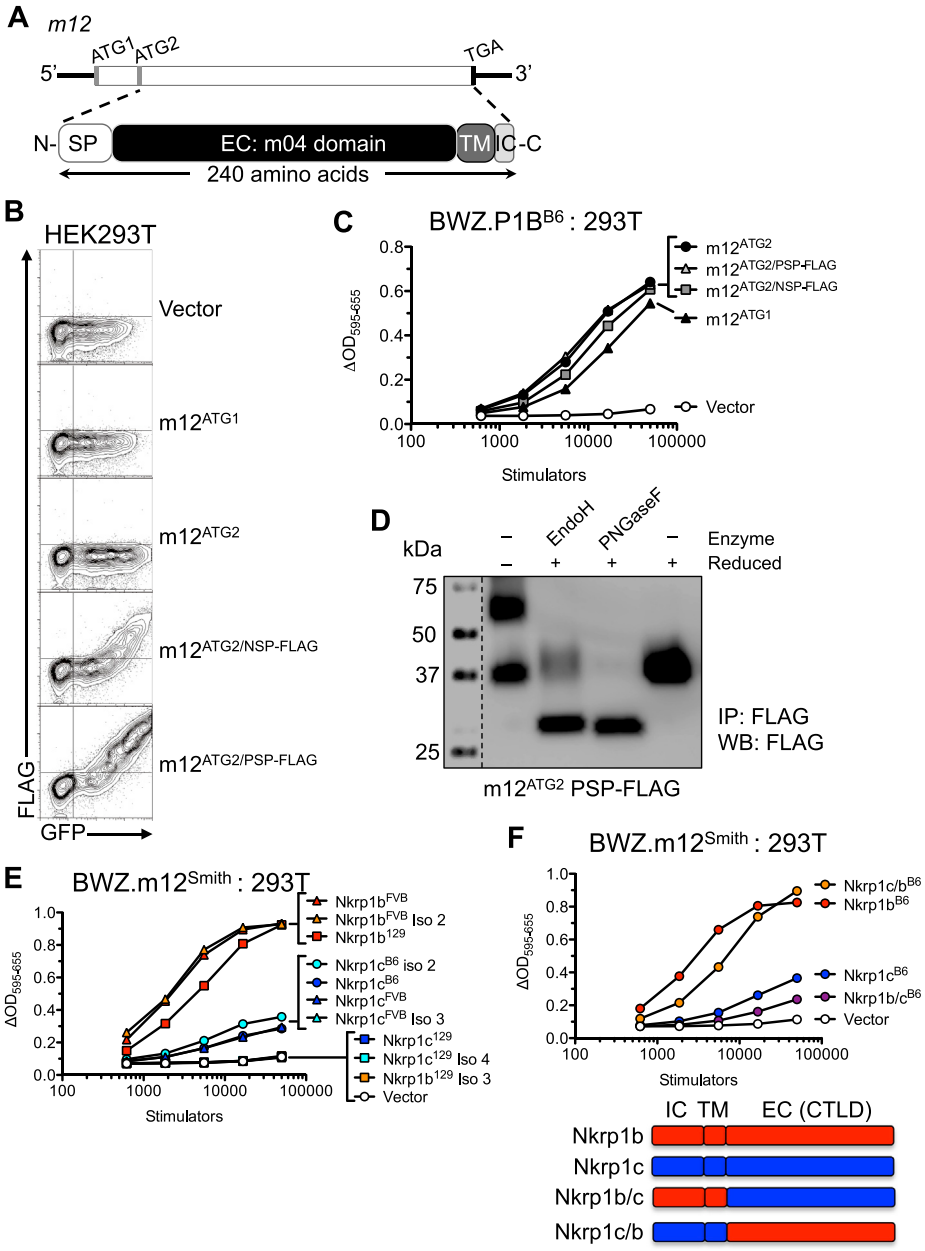

Figure S2. The MCMV m12 Gene Product Is a Glycosylated Type-I Transmembrane Protein Capable of Interacting with Numerous NKR-P1B/C Isoforms, Related to Figures 1 and 2

(A) Structural diagram of the m12 gene with 2 translational start sites (ATG1/2) and TGA stop codon labeled (top) and domain structure of the m12 protein (bottom). SP, signal peptide; EC, extracellular m04-like domain; TM, transmembrane domain; IC, intracellular domain.

(B) Cell surface expression of native and N-terminally FLAG-tagged m12 (NSP, native signal peptide; PSP, preprotrypsin signal peptide) constructs cloned into pIRES2-EGFP and transfected into HEK293T.

(C) Stimulation of BWZ.NKR-P1B^{B6} cells by different m12 constructs.

(D) Immunoprecipitation of m12$^{ATG2/PSP-FLAG}$ transfected into HEK293T cells, isolated under different conditions, and immunoblotted for FLAG expression; a dashed line indicates the merged white light image (molecular weight marker lane) with the ECL image (Western blot lanes). Data are representative of at least 3 independent experiments.

(E) Nkrp1 splice isoforms were cloned into pIRES2-EGFP using cDNA from B6, 129, and FVB splenic LAK, transfected into HEK293T cells, and used as stimulators for BWZ.m12^{Smith} reporters.

(F) Intracellular (IC) and extracellular (EC) domain swaps of NKR-P1B^{B6} and NKR-P1C^{B6} were constructed and tested for their ability to stimulate BWZ.m12^{Smith} reporters upon transfection into HEK293T. Data are representative of at least 2 independent experiments.

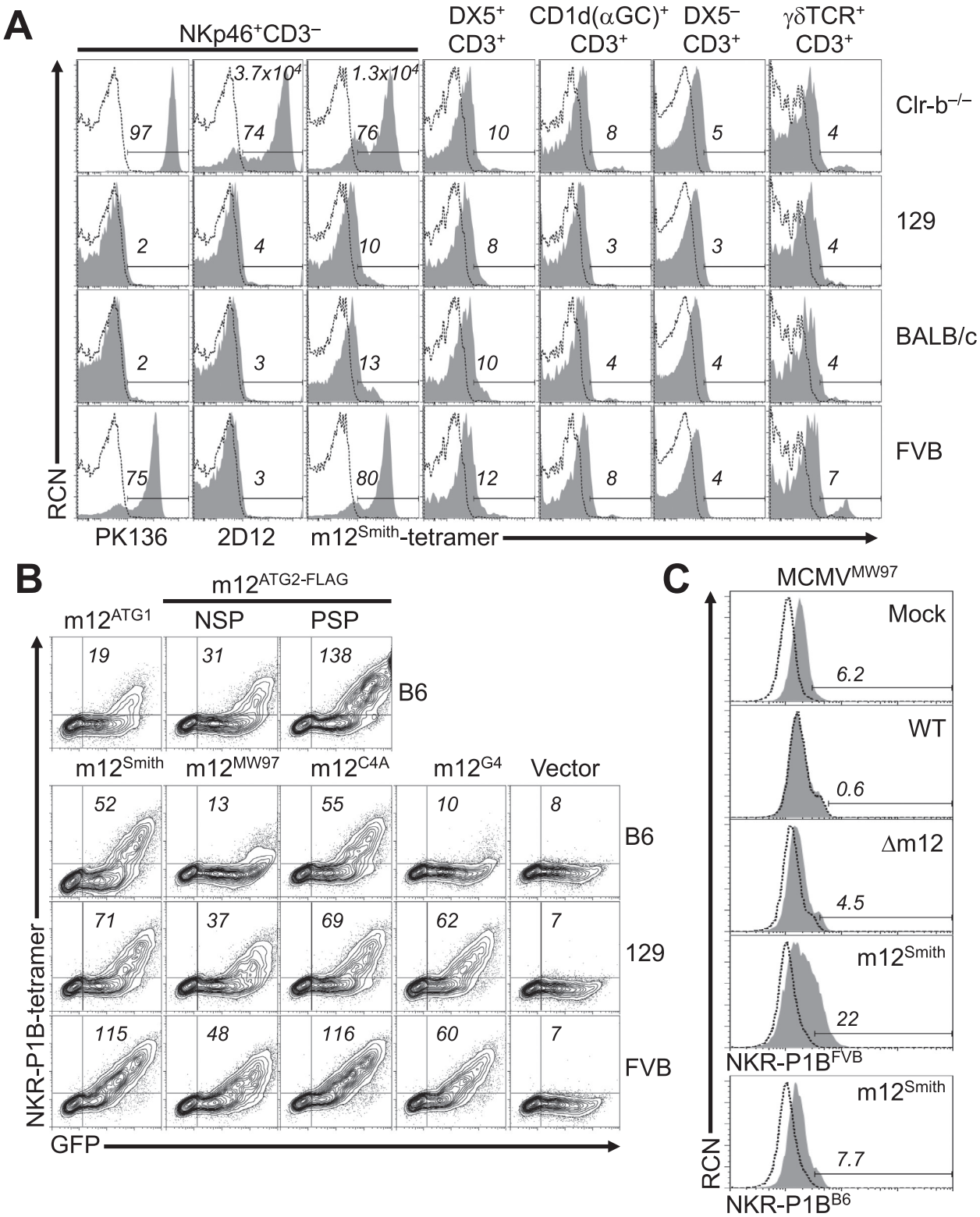

Figure S3. Direct NKR-P1 and m12 Interactions Revealed by Tetramer Staining of Ex Vivo Immune Cell Subsets, Transfectants, and MCMV-Infected Cells, Related to Figure 3

(A) $m12^{Smith}$ tetramers were used to stain ex vivo splenic immune cell subsets from distinct mouse strains. Numbers above gates represent percentage of gated positive cells; numbers at top right corner represent MFI of positive cells for 2D12 and m12-tetramer staining to highlight a ~2-fold increase in NKR-P1B levels on

(legend continued on next page)

B6.*Clr-b*$^{-/-}$ NK cells relative to WT B6 NK cells (see Figure 3F). Gated positive cells (shaded histograms) are shown compared to the corresponding B6 mouse FMO negative control samples (dashed lines).

(B) NKR-P1B tetramer staining of HEK293T cells transfected with m12 variants. Numbers represent mean fluorescence intensity.

(C) NKR-P1B tetramer staining of MCMV-infected NIH 3T3 cells. Numbers represent percentage of gated positive cells.

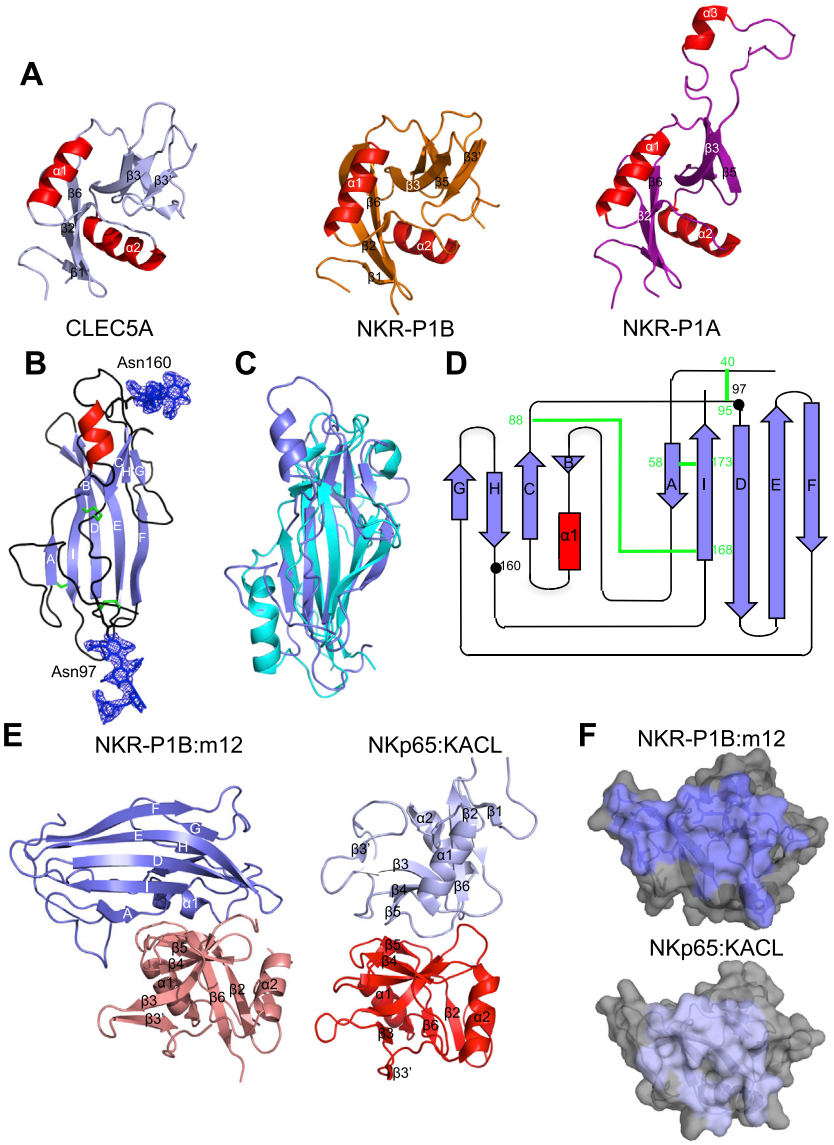

Figure S4. Structure of NKR-P1B and m12 and Comparison to Known Structures and Docking Modes, Related to Figure 4

(A) Comparison of the NKR-P1B C-type lectin-like domain with that of CLEC5A (PDB ID 2YHF) and NKR-P1A (PDB ID 3M9Z).

(B) Overview of the m12 ectodomain in cartoon representation. β-strands are colored blue; α-helices are red; and loop regions are shown in black. Cysteine residues that form intra-molecular disulfide bonds are shown as green sticks. The refined $2F_o$-F_c electron density map for the attached sugar moieties (blue sticks) is shown as a blue mesh and contoured at 3σ.

(C) Alignment of the $m12^{Smith}$ (blue) and $m04^{G4}$ ectodomains (cyan) (PDB ID 4PN6).

(D) Schematic representation of the m12 ectodomain fold, colored as in (B). Amino acid residues involved in disulfide bonding and sugar attachment are labeled in green and black respectively.

(E) Side-by-side comparison of NKR-P1B (salmon) bound to m12 (blue) and NKp65 (red) bound to KACL (light blue) (PDB ID 4IOP). Structures are shown in the same orientation with respect to the receptor.

(F) Top view showing the footprint made by each ligand on its corresponding receptor. The molecular surface of the receptors is colored gray, with the residues that contact the ligand colored blue.

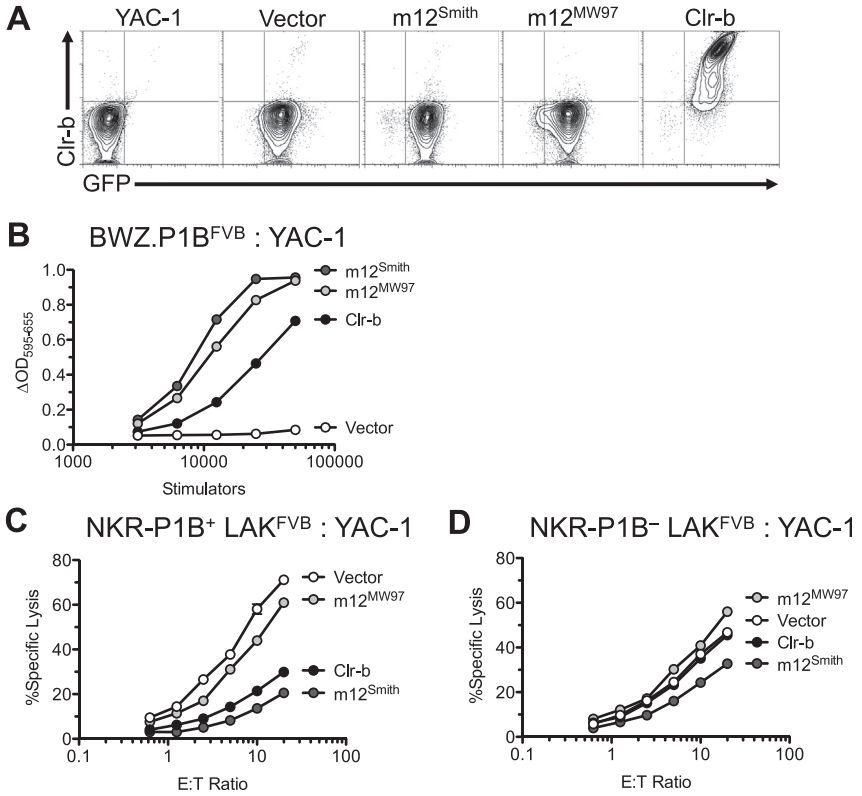

Figure S5. Generation and Characterization of YAC-1 Transductants, Related to Figure 5

(A and B) YAC-1 cells were transduced with pMSCV2.2-IRES-EGFP retrovirus encoding $m12^{Smith}$, $m12^{MW97}$, Clr-b, or parental empty vector and sorted for matching GFP levels. Stable YAC-1 transductants were (A) analyzed by flow cytometry for Clr-b expression and (B) used as stimulator cells for BWZ.NKR-$P1B^{FVB}$ reporter cells.

(C and D) Stable YAC-1 transductants were used as target cells in ^{51}Cr-release cytotoxicity assays for (C) NKR-$P1B^{+}$ or (D) NKR-$P1B^{-}$ FVB-strain splenic NK-LAK effector cells. Mean±SEM are shown. Data are representative of at least 2 independent experiments.

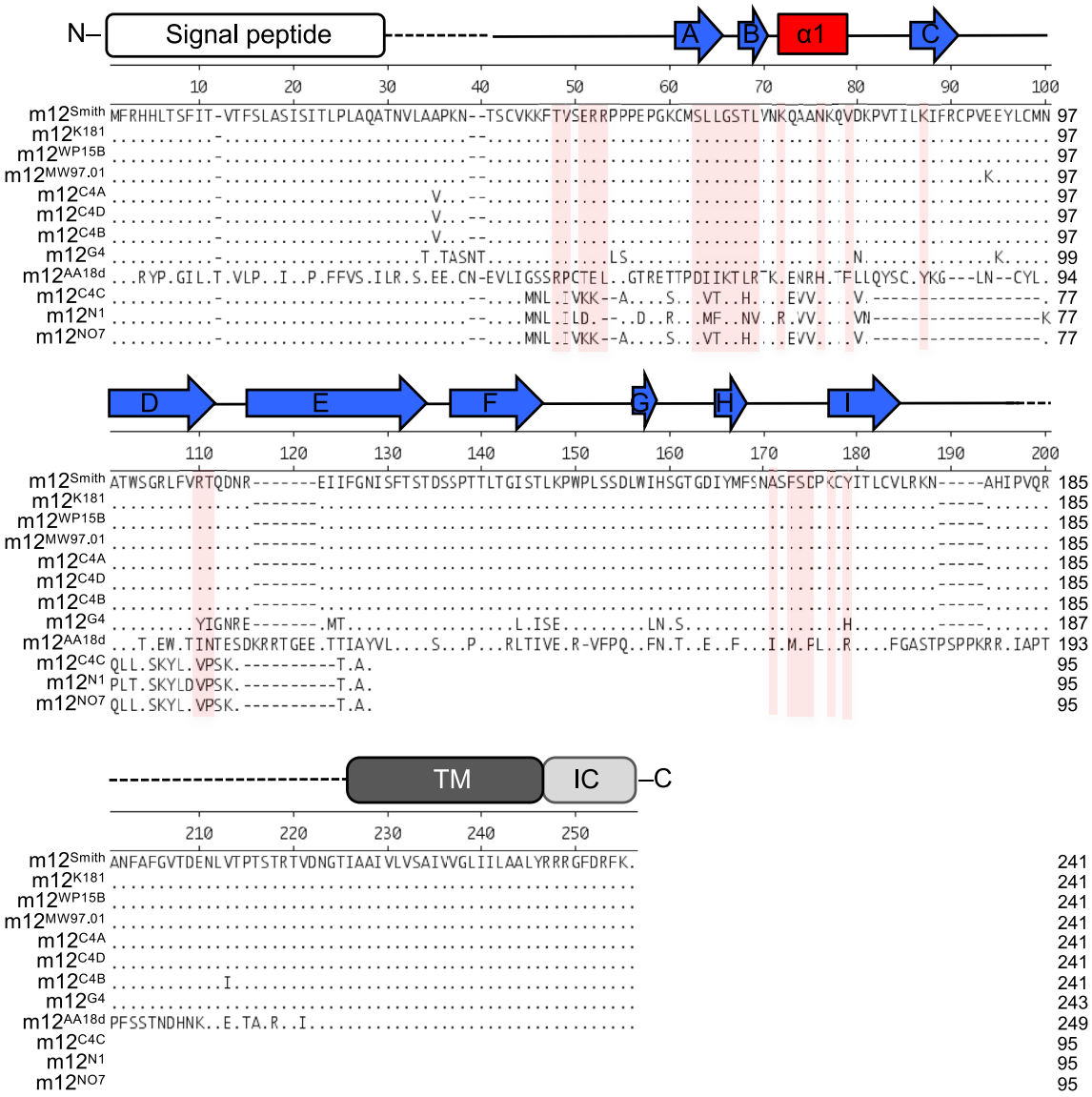

Figure S6. Protein Alignments of m12 Variants from Sequenced MCMV Genomes, Related to Figure 6

Amino acid sequences of m12 from laboratory MCMV strains (Smith, K181, and MW97.01) and wild-derived MCMV variants (WP15B, C4A, C4B, C4C, C4D, G4, AA18d, N1, and NO7) were aligned using ClustalW. The protein domains and secondary structure elements are labeled above the amino acid sequences; TM, transmembrane domain; IC, intracellular domain; blue arrows, β-sheets; red rectangles, α-helices. Dashed lines represent regions not visible in the crystal structure. m12 residues that make contacts to NKR-P1B[B6] are highlighted with a pink background.

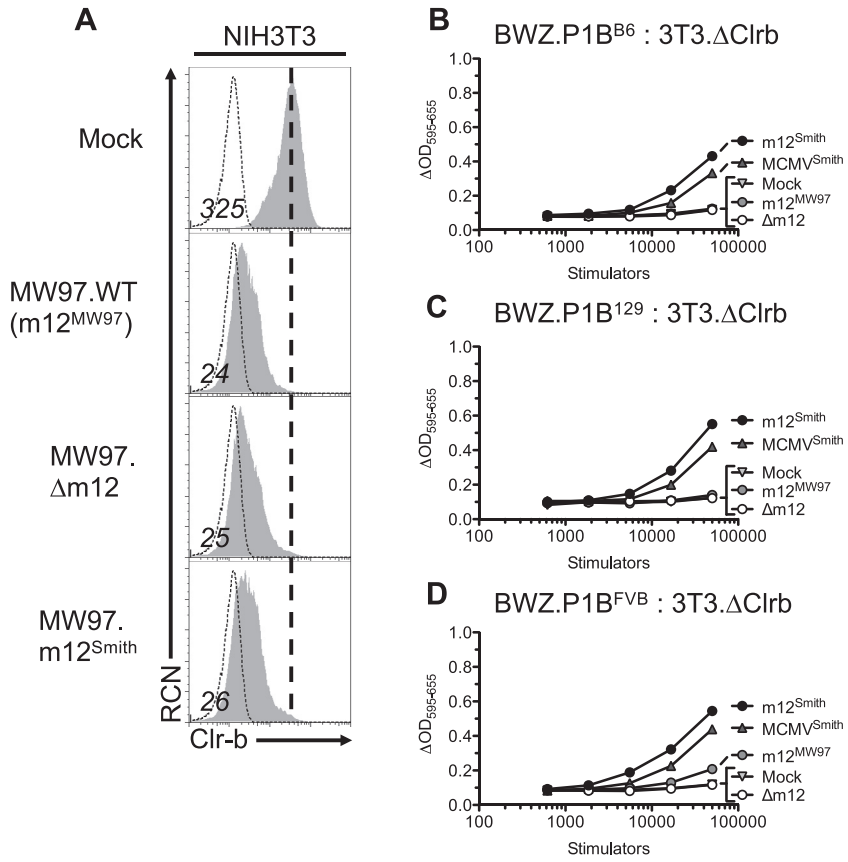

Figure S7. Parental MW97-Derived m12 Variants Retain Ability to Downregulate Clr-b and Differentially Stimulate NKR-P1B Reporters, Related to Figure 7

(A–D) NIH 3T3 cells were infected with MCMV m12 variants (MOI = 0.5) and assessed for cell surface Clr-b expression 24 hr post-infection by flow cytometry. Numbers correspond to Clr-b MFI; shaded histograms, Clr-b staining; dashed lines, secondary reagent alone. NIH 3T3.ΔClr-b fibroblasts were infected with MCMV variants and used as stimulators for (B) BWZ.NKR-P1B^{B6}, (C) BWZ.NKR-P1B^{129}, and (D) BWZ.NKR-P1B^{FVB} reporter cells.